# Refinement of Supersonic Inlets for Mach 1.4 to 2.0

John W. Slater[1]
*John H. Glenn Research Center, Cleveland, Ohio, 44135, USA*

**The design and analysis of several external-compression inlets for freestream Mach numbers of Mach 1.4, 1.7, and 2.0 were refined from earlier designs to improve their aerodynamic performance and explore additional design aspects. The types of inlets included axisymmetric pitot, axisymmetric spike, two-dimensional, two-dimensional bifurcated, and streamline-traced inlets. The inlets were designed as isolated from the airframe with freestream conditions, engine-face geometry, and flow rates established from a reference NASA commercial supersonic aircraft concept. The inlets were designed using the NASA Supersonic Inlet Design and Analysis (SUPIN) Tool and the inlet performance was obtained from computational fluid dynamics (CFD) simulations. The study compared the physical dimensions and aerodynamic performance of the inlets at the on-design cruise conditions and off-design conditions involving angle-of-attack and Mach number variations. The study provides data to inform the selection of inlets for commercial supersonic aircraft.**

## Nomenclature

| | | |
|---|---|---|
| $A$ | = | Cross-sectional area |
| $\alpha_0$ | = | Angle-of-attack |
| $\beta_{stex}$ | = | Angle of the outflow conical shock wave of the Busemann flowfield |
| $C_{Dwave}$ | = | Cowl exterior wave drag coefficient |
| $D_{hub}$ | = | Diameter of the hub or spinner at the engine face |
| $D_{noz}$ | = | Diameter of the throat of the outflow nozzle |
| $\Delta y_{focal}$ | = | Vertical offset of the focal point from the cowl lip point |
| DPC/P | = | Circumferential total pressure distortion intensity |
| DPR/P | = | Radial total pressure distortion intensity |
| $h_0$ | = | Altitude for the freestream |
| $h_{plen}$ | = | Height of the bleed slot plenum |
| $L_{cb1sh}$ | = | Length from the end of the external supersonic diffuser to the start of the shoulder / bleed slot |
| $L_{cwcl}$ | = | Length of cowl interior just downstream of the cowl lip interior |
| $L_{exd}$ | = | Length of the external supersonic diffuser |
| $L_{inlet}$ | = | Length of the inlet |
| $L_{plen}$ | = | Length of the bleed slot plenum |
| $L_{shSD}$ | = | Length from the end of the shoulder / bleed slot to the start of the subsonic diffuser |
| $L_{slot}$ | = | Length of the shoulder / bleed slot |
| $L_{subd}$ | = | Length of the subsonic diffuser |
| $L_{thrt}$ | = | Length of the throat section |
| $M$ | = | Mach number |
| $M_{EX}$ | = | Supersonic Mach number at the end of the external supersonic diffuser |
| $M_{stex}$ | = | Mach number downstream of the Busemann outflow conical shock wave |
| $N_{stgs}$ | = | Number of stages for the external supersonic diffuser |
| $p_t$ | = | Total pressure |
| $S_{comp}$ | = | Surface area of compressive surfaces of an inlet |

[1] Research Aerospace Engineer, Propulsion Division / Inlets and Nozzles Branch, AIAA Associate Fellow.

| | | |
|---|---|---|
| $S_{cwexx}$ | = | Surface area of a cowl exterior projected to an axial plane |
| $S_{inlet}$ | = | Total surface area of an inlet |
| $\theta_{clex}$ | = | Slope of cowl lip exterior point |
| $\theta_{eqSD}$ | = | Equivalent conical angle for the subsonic diffuser |
| $\theta_{stle}$ | = | Slope of leading edge of the streamline-traced surface |
| $\theta_{stg\#}$ | = | Slopes for the stages of the external supersonic diffuser with # = (1,2,3) |
| $T_t$ | = | Total temperature |
| $w_{cap}$ | = | Width of the capture cross-section for the two-dimensional inlets |
| $W$ | = | Flow rate |
| $W_{bleed}$ | = | Flow rate of bleed |
| $W_{C2}$ | = | Altitude-adjusted corrected flow rate at the engine face |
| $W_{spillage}$ | = | Flow rate of supersonic and subsonic spillage |
| $x, y, z$ | = | Cartesian coordinates |
| $(x,y)_2$ | = | Planar coordinates of the center point of the engine face |
| $(x,y,\theta)_{cb1}$ | = | Planar coordinates and slope on the centerbody at the endpoint of the external supersonic diffuser |
| $(x,y,\theta)_{cbTS}$ | = | Planar coordinates and slope on the centerbody at the shoulder point |
| $(x,y,\theta)_{cbSD}$ | = | Planar coordinates and slope on the centerbody at the start of the subsonic diffuser |
| $(x,y,\theta)_{clip}$ | = | Planar coordinates and slope of the cowl lip point |
| $(x,y,\theta)_{clin}$ | = | Planar coordinates and slope at the cowl lip interior point |
| $(x,y,\theta)_{cwTS}$ | = | Planar coordinates and slope on the cowl interior at the shoulder point |
| $(x,y,\theta)_{cwSD}$ | = | Planar coordinates and slope on the cowl interior at the start of the subsonic diffuser |
| $(x,y,\theta)_{SD}$ | = | Planar coordinates and slope of center point at start of the subsonic diffuser |
| $x_{stg\#}$ | = | $x$-coordinates for the endpoints for the stages of the external supersonic diffuser with # = (1,2,3) |
| $y_{inlet}$ | = | $y$-coordinate of inlet axis |
| $(\ )_0$ | = | Freestream property |
| $(\ )_1$ | = | Property at the cowl lip / inlet entrance station |
| $(\ )_2$ | = | Property at the engine-face station |
| $(\ )_{cap}$ | = | Property associated with the reference capture area |
| $(\ )_{ref}$ | = | Property associated with the reference inlet |
| $(\ )_{SD}$ | = | Property at station SD, start of the subsonic diffuser |
| $(\ )_{TS}$ | = | Property at station TS, shoulder of the throat section |

## I. Introduction

Commercial supersonic aircraft are characterized by a supersonic cruise segment that encompasses most of the flight time of the aircraft and that can involve a duration of hours at a near-constant supersonic cruise speed. Thus, the supersonic cruise conditions form the key reference point for the aircraft design. Recent efforts for the design of a commercial supersonic aircraft have focused on relatively smaller aircraft for 12 to 80 passengers cruising between Mach 1.4 to 2.0. This speed region provides travel at about twice the speed of current subsonic commercial aircraft while reducing thermal, material, and propulsion challenges associated with flight above Mach 2.

A commercial supersonic aircraft requires an efficient propulsion systems consisting of the inlet, turbofan engine, and nozzle. The propulsion system should be well integrated with the airframe to provide the necessary thrust while minimizing drag throughout the flight of the aircraft. The focus of this paper is on the aerodynamic design of the inlet. The primary task of the inlet is to capture and process the airflow required by the engine in the most efficient and stable manner possible.

At supersonic speeds the processing of the captured inlet flow involves decelerating supersonic flow to subsonic conditions required by the turbofan engine. The deceleration of this flow also results in compression of the flow which contributes to the compression for the propulsion cycle. The deceleration and compression of supersonic flow is performed using a shock wave system that at its outflow creates subsonic flow which is further decelerated by the inlet subsonic diffuser to achieve the subsonic flow desired by the engine. For cruise Mach numbers at or below 2.0, a shock wave system external to the inlet interior duct is regarded as the appropriate choice based on the desire for an efficient yet stable shock wave system. Thus, the inlets studied and discussed within this paper are external-compression inlets.

Several types of supersonic, external-compression inlets are possible and those types include the axisymmetric pitot, axisymmetric-spike, two-dimensional, two-dimensional bifurcated-duct, and streamline-traced inlets. These type of inlets are primarily distinguished by the character of the shock wave system and deceleration of supersonic flow. The choice of inlet type affects both the aerodynamic performance and stability of the inlet flow, as well as the physical dimensions (i.e., lengths, diameters, surface areas) of the inlet. In addition to maximum aerodynamic efficiency and stability, a goal of the inlet design is to minimize the physical dimensions of the inlet to keep the weight and aerodynamic drag at a minimum.

The study described in this paper examined the physical dimensions and aerodynamic performance for the various inlet types designed for flight Mach numbers of Mach 1.4, 1.7, and 2.0. The design of an inlet requires specification of the flow conditions approaching the inlet and the physical dimensions and flow rate at the engine face, which is the interface of the inlet with the engine. For this study, this information was obtained from consideration of the NASA Supersonic Technology Concept Aeroplane (STCA) [1]. The STCA is a 55-ton business-class airplane concept powered by three turbofan engines and designed to perform transatlantic flights with 8 passengers at a cruise of Mach 1.4. The STCA study also included a conceptual design of a low-bypass turbofan engine. It was assumed in this study that the inlets would be integrated with the airframe such that the flow approaching the inlet would be uniform and not adversely affected by the inlet-airframe integration. This assumption allowed the inlets of this study to be designed as isolated from the airframe. Further, the flow approaching the inlet was assumed to be the freestream conditions approaching the aircraft. The aerodynamic performance of the inlet was characterized by the flow rates, the total-pressure recovery and distortion at the engine face, and the wave drag.

The current study built upon previous inlet design studies performed by the author and colleagues. Reference [2] studied two-dimensional inlets for the Mach range of interest. Reference [3] discussed the design of an axisymmetric spike inlet for Mach 1.4. References [4] and [5] discussed the design of a streamline-traced, external-compression inlet for Mach 1.7 and 2.0, respectively. Reference [6] discussed a study of the two-dimensional inlet for the Concorde. Reference [7] explored the range of inlet types for Mach 1.4, 1.7, and 2.0 and compared their inlet performance and physical characteristics. Reference [8] refined the axisymmetric spike inlets of Ref. [7] and explored off-design and subsonic conditions for the inlets. This included analysis of the inlets at take-off and approach-to-landing conditions in which auxiliary intakes were used. The current study refines some of the inlets of Ref. [7] and explores in greater depth the two-dimensional bifurcated and streamline-traced inlets for Mach 1.7 and 2.0. The current study also further explores some off-design performance of the refined inlets.

A description of the inlet types included within the study of this paper is presented in Section II. Geometry models are described for the design of the external supersonic diffusers, throat section, and subsonic diffuser and the important design factors are identified. The design of the inlets was facilitated using the NASA Supersonic Inlet Design and Analysis (SUPIN) Tool [9], which is also briefly described in Section II. While SUPIN provided estimates of the inlet aerodynamic performance, computational fluid dynamics (CFD) simulations were used to obtain higher fidelity estimates of the inlet performance. Section III describes the computational grids and methods used for the CFD simulations. Section IV discusses the aerodynamic performance and physical characteristics of the refined inlets. The physical dimensions and aerodynamic performance of the inlets are presented and compared. The characteristic curves for the variations of the total pressure recovery and distortion as the engine flow ratio was varied are also presented. This includes curves from variation of angle-of-attack and Mach number about the cruise conditions. This papers concludes with some guidance for the selection and design of inlets for future commercial supersonic aircraft.

## II. Descriptions of the Inlets

This section describes the physical features, freestream and engine-face conditions, and geometry models for the five inlet types of the study.

### A. Inlet Types

This study explored the design of axisymmetric pitot, axisymmetric spike, two-dimensional, two-dimensional bifurcated, and streamline-traced inlets for commercial supersonic aircraft using the NASA STCA [1] as a reference aircraft. Figure 1 shows images of the five inlet types. The inlets shown are external-compression inlets designed for the Mach 1.7 inflow conditions with the STCA turbofan engine at their outflow.

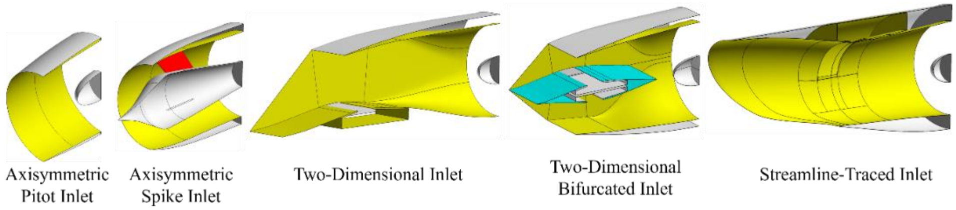


**Figure 1. Types of supersonic external-compression inlets as designed for Mach 1.7.**

The inlet types primarily differ in the nature of the supersonic compression and shock wave system. The axisymmetric pitot inlet uses a normal shock wave at its leading edge to decelerate the supersonic flow approaching the inlet to subsonic speeds for capture by the inlet duct. The axisymmetric spike inlet uses the external spike to create conical shock wave and Mach waves to decelerate the supersonic flow. An annular normal shock wave at the start of the internal ducting then decelerates the flow to subsonic conditions for entry into the interior ducting of the inlet. The two-dimensional inlets use planar oblique shock and Mach waves on the exterior ramps. A planar normal shock wave then decelerates the flow to subsonic conditions. Both the axisymmetric spike and two-dimensional inlets turn the flow outward with respect to the axis of the turbofan engine. The streamline-traced inlet uses a system of three-dimensional shock and Mach waves to turn the flow inward with respect to the axis of the engine. A strong, oblique shock wave then decelerates the flow to subsonic conditions. Further discussion of the supersonic compression flowfields will be presented below in the discussion of the external supersonic diffusers.

The general features of the inlets are represented in Fig. 2. Figure 2a. shows the two-dimensional inlet for Mach 1.7 and represents the features and stations of the axisymmetric spike and two-dimensional inlets. Figure 2b. shows the features and stations for the streamline-traced inlet for Mach 1.7. The main components of the inlets are the external supersonic diffuser, throat section, and subsonic diffuser. The axisymmetric pitot inlet does not have an external supersonic diffuser. The nose is the forward-most point on the inlet and the start of the external supersonic diffuser. The cowl lip starts the internal ducting of the inlet, which consists of the throat section and subsonic diffuser. For the streamline-traced inlet, the cowl lip is the downstream point of the leading edge of the inlet. The end and outflow boundary of the inlet is the engine face at which the subsonic diffuser interfaces with the turbofan engine. The engine face includes a spinner about the hub of the turbofan engine. The circular engine face and spinner cross-section creates an annular cross-section for flow into the fan stage of the engine. The inlet is assumed to be symmetric with respect to a vertical plane passing through the axis of the engine face. The cowl exterior wraps about the inlet. References [2-9] provide more detailed descriptions of the various inlets.

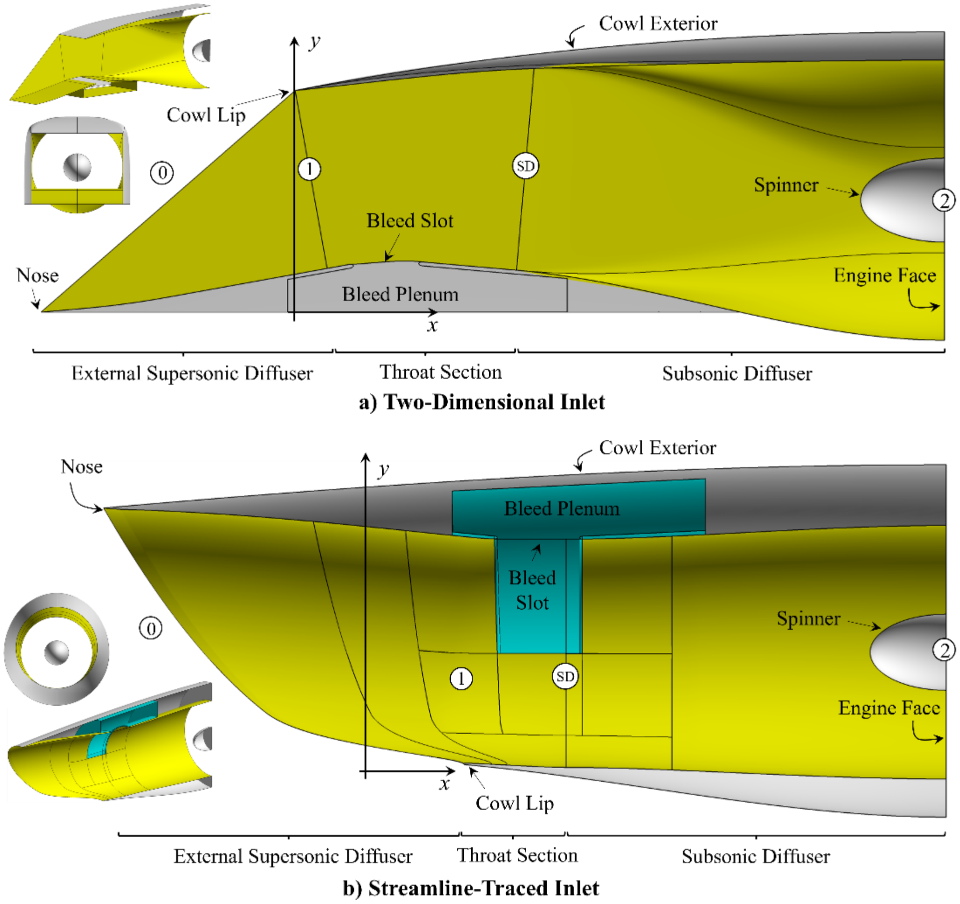


**Figure 2. Description and stations of the inlets.**

For the inlets, the $x$-axis is in the horizontal direction. For the axisymmetric inlets, the $x$-axis is along the axis-of-symmetry. For the two-dimensional inlet, $x$-axis is passes through the leading edge of the external supersonic diffuser. For the streamline-traced inlet, the $x$-axis coincides with the axis-of-symmetry of the parent flowfield through which the streamline tracing is performed. The $y$-axis is vertical with a positive orientation upward. For the axisymmetric and two-dimensional inlets, the $y$-axis passes through the cowl lip point. For the streamline-traced inlet, the $y$-axis is at the origin of the parent flowfield. The $z$-axis completes the right-hand rule with its origin on the plane-of-symmetry.

The numeric stations 0, 1, and 2 shown in Fig. 2 correspond to the freestream, cowl lip or entrance to the internal ducting, and engine face stations, respectively, and are consistent with the SAE propulsion system stations [10]. Station SD is an additional station that denotes the start of the subsonic diffuser. For an external-compression inlet, subsonic flow is expected at or shortly downstream of station 1. Thus, the location of station SD is based on the geometric modeling for the inlet that distinguishes between the throat section and subsonic diffuser.

The two-dimensional and streamline-traced inlets can feature a bleed slot located at the shoulder of the inlet, as shown in Fig. 2. The shoulder point is defined within the throat section where the inlet interior surface has a zero slope and exhibits a "hump" shape.

### B. Freestream

The design of an inlet requires an understanding of the flow approaching the inlet. The approach flow forms the upstream boundary conditions to the inlet design problem. For the current study, the inlets were considered isolated without interactions with the airframe, and so, the flow approaching the inlet was designated to be at station 0 and at the uniform freestream conditions. The freestream conditions include the Mach number ($M_0$), altitude ($h_0$), angle-of-attack ($\alpha_0$), and angle-of-sideslip ($\beta_0$). For a specified altitude, the US Standard Atmosphere was used to find the static pressure and temperature that defined the thermodynamic state of the freestream. The angle-of-attack specifies the incidence of the inlet axis with the freestream. For this study, $\beta_0 = 0$. Table 1 lists the altitudes assumed for each of the three freestream Mach numbers along with the freestream total pressures ($p_{t0}$) and total temperatures ($T_{t0}$).

**Table 1. Freestream and engine-face conditions.**

| $M_0$ | $h_0$ (ft) | $p_{t0}$ (psi) | $T_{t0}$ (°R) | $W_{C2}$ (lbm/s) | $M_2$ |
|---|---|---|---|---|---|
| 1.4 | 50000 | 5.353 | 542.84 | 413 | 0.663 |
| 1.7 | 55000 | 6.529 | 615.37 | 383 | 0.581 |
| 2.0 | 60000 | 8.139 | 389.97 | 353 | 0.514 |

### C. Engine Face

The engine face forms the downstream boundary condition to the inlet design problem with the specification of the engine face geometry and the flow rate. The turbofan engine used for the inlet designs is that of the concept engine for the STCA [1] and is based on publicly available data for the CFM International CFM56-7B engine. The engine has a single-stage fan with a smaller diameter than that of the CFM56, but with a larger pressure ratio. The low-pressure compressor was removed to compensate for the higher ram pressure and temperatures of supersonic flight.

The engine face was modeled as an annular cross-section oriented perpendicular to the $x$-axis with a spinner at the center. The engine face had a diameter of $D_2 = 3.625$ feet with a spinner with a hub-to-tip ratio of $D_{hub}/D_2 = 0.3$. The profile of the spinner was elliptical with an aspect ratio (i.e., length-to-diameter) of 2.0. The annular cross-sectional area of the engine face ($A_2$) was formed by the circular engine face and spinner hub diameter and has cross-sectional area of $A_2 = 9.3918$ ft$^2$. Figures 1 and 2 show shapes for the engine face and spinner. The center of the engine face was positioned on the vertical plane of inlet symmetry (i.e., $z_2 = 0$ ft). The axial placement of the engine face ($x_2$) depended on the overall length of the inlet. The vertical placement of the engine face ($y_2$) depended on the type of inlet. For the axisymmetric inlets, the engine axis was coincident with the inlet axis-of-symmetry. For the two-dimensional, bifurcated inlet, the engine axis was coincident with the inlet axis located on the mirror plan of the two halves of the inlet. For the two-dimensional and streamline-traced inlets, the engine axis could be offset in the vertical direction from the inlet axis. Since the inlets were isolated, the offset was chosen either to reduce the local slope variations of the internal surface of the subsonic diffuser or reduce the forward-facing surface area of the cowl exterior, which can reduce cowl wave drag.

The engine flow rate was specified by the engine-face corrected flow rate ($W_{C2}$), which was set by the desired level of thrust as part of the mission profile of the aircraft. The values of $W_{C2}$ used for the inlet designs for each freestream Mach number ($M_0$) are listed in Table 1. The engine-face corrected flow rate decreased with increased freestream Mach number in response to limits on the engine maximum temperature. Ref. [1] only provided data for the engine of the STCA aircraft up to $M_0 = 1.4$. The values of $W_{C2}$ listed in Table 1 for $M_0 = 1.7$ and 2.0 were obtained using a linear extrapolation of the STCA engine data for $M_0$ = 1.3 and 1.4. The engine-face corrected flow rate corresponded to an engine-face mass-averaged Mach number ($M_2$), which are also listed in Table 1.

### D. External Supersonic Diffuser

The external supersonic diffuser uses shock and Mach waves to form a compressive, supersonic flowfield in which the supersonic freestream Mach number ($M_0$) is decelerated to a lower supersonic Mach number ($M_{EX}$) at the end of the external supersonic diffuser. Thus, $M_{EX}$ is an important design factor for the external supersonic diffuser and values for the diffuser ranged from $1.25 \leq M_{EX} \leq 1.40$. A key consideration in selecting $M_{EX}$ is to limit the static pressure rise across the terminal shock wave to avoid or limit separation of the boundary layer on the diffuser surfaces due to interactions with the terminal shock wave.

#### *1. External Supersonic Diffusers for the Axisymmetric Spike and Two-Dimensional Inlets*

The external supersonic diffuser for the axisymmetric spike and two-dimensional inlets performs the supersonic compression using shock and Mach waves that are formed due to the outward turning of the surfaces of the external supersonic diffuser. An important design factor for the external supersonic diffuser is the number of stages ($N_{stgs}$). For the $M_0$ = 1.4 inlets, only one stage ($N_{stgs}$ = 1) was used due to the low level of compression needed. For the $M_0$ = 1.7 and 2.0 inlets, three stages ($N_{stgs}$ = 3) were used to reduce the total pressure losses through the diffuser. Figure 3 shows the external supersonic diffuser for a two-dimensional inlet with three stages. The external supersonic diffuser for an axisymmetric spike inlet has a similar form, but with conical stages. The first stage is always a cone or ramp with a deflection with respect to the x-axis of $\theta_{stg1}$, which forms an oblique shock wave at the nose of the inlet. For the case of $N_{stgs}$ = 3, the second stage could be curved to create a series of compressive Mach waves that are focused on the cowl lip and form an isentropic compression. The selection of $N_{stgs}$ and $M_{EX}$ establishes the slopes of each stage ($\theta_{stg\#}$). For two-dimensional inlets, the Oswatitsch condition as described in Ref. [9] is used to compute the slopes such that the decrease in the total pressure is the same across all the shock waves. The stage deflections and local Mach numbers determine the wave angles. The ends of the stages are denoted by the coordinates $x_{stg1}$, $x_{stg2}$, and $x_{stg3}$. These coordinates are established by specification of the focal points of the wave. The placement of the focal points involves a vertical displacement ($\Delta y_{focal}$) from the cowl lip point. The focal points of all waves were specified for this study to be the cowl lip ($\Delta y_{focal}$ = 0). This implies the diffuser creates no supersonic spillage ($W_{spillage}/W_{cap}$ = 0) past the cowl lip. If some small amount of supersonic spillage is desired in the inlet, then the focal point could be specified to be located above the cowl lip. The length of the external supersonic diffuser is defined as $L_{exd} = x_{stg3} - \underline{x}_{nose}$.

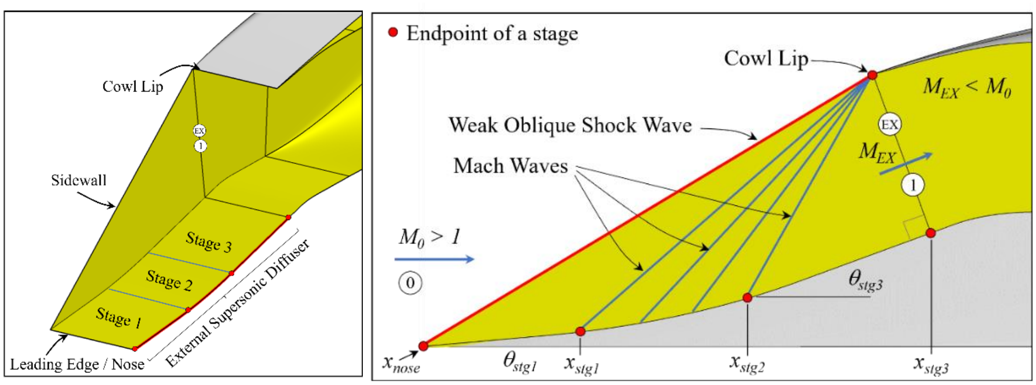


**Figure 3. Geometry model of the external supersonic diffuser for a two-dimensional inlet.**

The surface of the external supersonic diffuser for the axisymmetric-spike inlet is formed by extruding the planar profile of the diffuser about the axis-of-symmetry. The reference capture area of the diffuser is circular and is defined by $A_{cap} = \pi\, y^2_{clip}$. Where $y_{clip}$ is the vertical distance from the nose to the cowl lip point. Similarly, the external supersonic diffuser for the two-dimensional inlets is formed by extruding the profile in the *z*-direction over a capture width of $w_{cap}$. The two-dimensional inlets of this study specified that the width of the rectangular capture cross-section was equal to the engine-face diameter, $w_{cap} = D_2$. The two-dimensional inlet has a planar sidewall created with a leading edge defined by a line from the nose to the cowl lip. Thus, the reference capture area of the two-dimensional inlets is rectangular with the reference capture area defined as $A_{cap} = w_{cap}\, y_{clip}$. The two-dimensional, bifurcated inlet involves a mirroring of the capture cross-section, and so $A_{cap} = 2\, w_{cap}\, y_{clip}$. The capture flow rate ($W_{cap}$) is computed with the freestream conditions and the area $A_{cap}$ and serves as the reference flow rate.

### 2. *External Supersonic Diffusers for Streamline-Traced Inlets*

The external supersonic diffusers of the streamline-traced inlets used three-dimensional surfaces that were formed through tracing streamlines through a compressive parent flowfield. The streamline-traced inlets for this study used the ICFA-Otto-Busemann parent flowfield as described in Ref. [11]. This parent flowfield imposes an initial oblique shock wave followed by isentropic Mach waves based on the axisymmetric Busemann flowfield. The geometry model is illustrated in Fig. 4. A leading-edge interior angle of $\theta_{stle}$ = -5 degrees creates the initial oblique shock wave. The internal conical flowfield A (ICFA) solution is solved for the initial portion of the diffuser. This flowfield is then matched to the axisymmetric Busemann flowfield that is comprised of Mach waves for isentropic compression. At the end of the Busemann flowfield, a strong conical shock wave decelerates the supersonic flow to the uniform, axial subsonic flow downstream of the shock wave with $M_{stex}$ = 0.9. A closed set of tracing curves placed in the downstream flow provide the starting points for the streamline tracing in the upstream direction. In Fig.4, the tracing curves form a circle to result in a circular cross-section for the external supersonic diffuser. The tracing curves are defined using distinct super-ellipses for the top and bottom tracing curves. The design study also explored the use of a top tracing curve that has a smaller vertical dimension than the circular curve, as well as an increase in the super-ellipse parameter to impose rounded corners. The result was a flatter upper surface for the external supersonic diffuser and cowl exterior and is referred to as the "flattop" streamline-traced inlet. Further details on the parent flowfield and the streamline tracing can be found in Ref. [9].

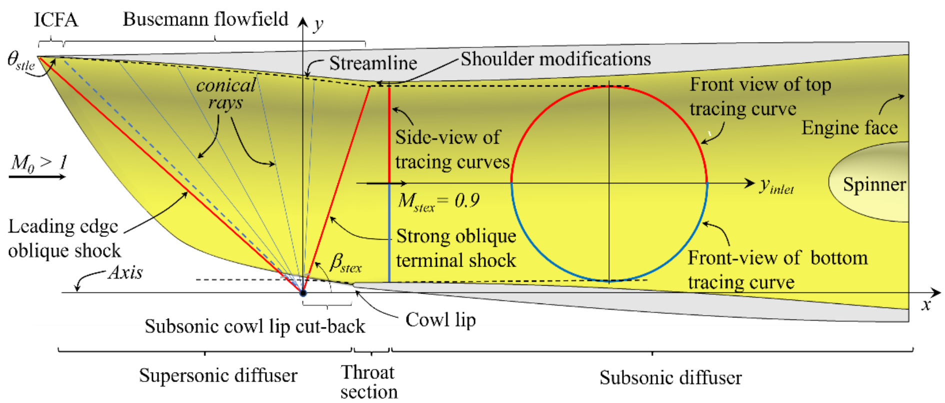


**Figure 4. Geometry model of the external supersonic diffuser for a streamline-traced inlet.**

## E. Throat Section

The throat section starts at station 1 and extends to the start of the subsonic diffuser at station SD. The role of the throat section is to enable the terminal shock wave structure to form subsonic flow while turning the flow toward the engine face. Geometry models are imposed to define the shape of the throat section in terms of a set of design factors.

### 1. *Geometry Model for the Throat Sections of the Axisymmetric Spike and Two-Dimensional Inlets*

The geometry models for the throat sections of axisymmetric spike and two-dimensional inlets are defined on a plane and involve the same set of design factors. The cross-sections through the throat section of axisymmetric spike inlets are annular while those of the two-dimensional inlets are rectangular. The width of the throat sections of two-dimensional inlets are fixed equal to the width of the inlet capture cross-section ($w_{cap}$). An illustration of the geometry model the throat section for a two-dimensional inlets is shown in Fig. 5. The design factors establish the planar profiles of the centerbody and the cowl interior through the throat section.

Point $(x,y)_{cb1}$ is the start of the throat section on the centerbody and is located on the line that intersects the cowl lip and is perpendicular to the end of the external supersonic diffuser. The slope of the centerbody at station 1 ($\theta_{cb1}$) is set to the slope of the last stage of the external supersonic diffuser. The profile of the centerbody through the throat section consists of three planar segments. The first segment is a line of length $L_{cb1sh}$ that starts at point $(x,y)_{cb1}$ and has a slope of $\theta_{cb1}$. The second segment consists of a non-uniform rational B-spline (NURBS) curve that forms the shoulder or bleed slot opening. This segment changes from its initial slope of $\theta_{cb1}$ to end slope of $\theta_{cbSD}$. The third segment is linear with a length of $L_{shSD}$ and slope of $\theta_{cbSD}$. The value of $\theta_{cbSD}$ is chosen such that the slope of the centerbody helps direct the flow at the end of the throat section toward the engine face.

The cowl interior starts at the cowl lip point, $(x,y)_{clip}$. The profile of the cowl lip is an ellipse with the cowl lip point $(x,y)_{clip}$ being the forward-most point. The major axis of the ellipse is oriented at an angle of $\theta_{clip}$. For a supersonic inlet, the ellipse is very small to approximate a nearly sharp cowl lip leading edge. The elliptical profile ends at the cowl lip interior point $(x,y)_{clin}$.

The profile for the cowl interior through the throat section consists of two segments. The first segment is linear with its start point at the cowl lip interior point $(x,y)_{clin}$ with a slope of $\theta_{clin} = \theta_{clip}$ and has a length of $L_{cwcl}$. The second segment is a planar NURBS curve that gradually changes the slope of the cowl interior profile from its initial slope of $\theta_{clin}$ to connect to the cowl interior point at station SD, $(x,y)_{cwSD}$ with a slope of $\theta_{cwSD}$. The value of $\theta_{cwSD}$ is chosen such that the slope of the cowl interior helps turn the flow toward the engine face while creating a smooth curve with the subsonic diffuser. The reference point $(x,y)_{cwTS}$ is located as the intersection point of the cowl interior profile and a vertical line that passes through point $(x,y)_{cbTS}$, defined as the point on the shoulder segment with a zero slope, or $\theta_{cbTS} = 0.0$. At the point $(x,y)_{cwTS}$, the cowl interior has a slope of $\theta_{cwTS}$. The location of point $(x,y)_{cwSD}$ is fully established with the specification of the cross-sectional area at station SD ($A_{SD}$) that is calculated using the area ratio $A_{SD}/A_1$. Alternatively, the Mach number at station SD ($M_{SD}$) can be specified and the area ratio computed based on area-Mach number relations accounting for the bleed flow extracted within the throat section.

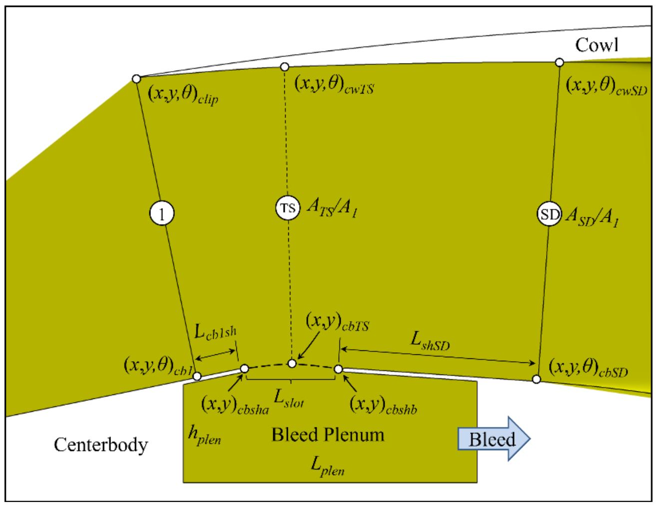


**Figure 5. Model of the throat section of a two-dimensional inlet.**

The throat section can accommodate a bleed slot. The slot opening occurs over the length of the shoulder and replaces the shoulder surface. A bleed slot plenum is constructed below the slot with a height ($h_{plen}$) and length ($L_{plen}$) to form a plenum that allows the slot bleed flow to reach essentially stagnant conditions.

At the design conditions for an external-compression supersonic inlet, the terminal shock wave is in the region of station 1. On the upstream side of the terminal shock wave, the Mach number is $M_{EX}$ and for the two-dimensional external supersonic diffuser, the flow is uniform along the upstream side of the terminal shock wave. Downstream of the terminal shock wave, the Mach number ($M_1$) is subsonic. The terminal shock wave may be a normal shock wave or a strong oblique shock wave. If the cowl lip interior angle is less than the flow angle, $\theta_{clip} < \theta_{cb1}$, and the static pressure downstream of the shock wave is not beyond a critical value, then a strong oblique shock wave can be established. With a strong oblique shock wave, some supersonic flow likely exists within the throat section and the throat section operates to further decelerate the flow to subsonic conditions prior to arrival of the flow at station SD. The strong oblique shock wave approach was used for the Concorde inlet as described in Ref. [6].

*2. Geometry Model for the Throat Sections of the Streamline-Traced Inlets*

The conical shock wave of the ICFA-Otto-Busemann flowfield produces outflow that by its nature is axial, and so the throat section of a streamline-traced inlet does not involve much turning of the flow. The cross-sections of the throat section are three-dimensional surfaces defined by the shapes of the tracing curves. Design factor specifies the axial length of the throat section ($L_{thrt}$) and the area ratio $A_{SD}/A_1$ of the throat section. Several design factors establish the shape of the cowl lip and their values can impose a cut-out by moving the cowl lip point downstream while specifying the dimensions and incidence of the cowl lip. For an external-compression inlet, the terminal shock wave wraps about the cowl lip and is a strong oblique shock wave to create subsonic flow downstream of the terminal shock wave. Thus, the design factors for the cowl lip can be set to influence the shape and flow through the terminal shock wave. Further details on the throat section for streamline-traced inlets can be found in Ref. [9].

### F. Subsonic Diffuser

The subsonic diffuser starts at station SD and ends at the engine-face station 2. The axial length of the subsonic diffuser is $L_{subd}$ is the primary design factor and is typically normalized by the engine-face diameter, or $L_{subd}/D_2$. As a general statement, a longer inlet helps the flow smoothly diffuse; however, a shorter inlet is typically desired to reduce the weight of the inlet. There also could be constraints placed on the design as to the length of the inlet.

Over the length, the subsonic diffuser transitions from the shape of the throat cross-section at station SD to a circular cross-section at station 2, which can be seen in the images of Fig. 1. For the two-dimensional inlets, the transition is from a rectangular cross-section at station SD to a annular cross-section at station 2, as illustrated in Fig. 6. The two-dimensional and streamline-traced inlets allow a vertical offset of the engine face to match the inlet up with the engine placement within the airframe. Within this study, the engine was placed mostly in line with the inlet axis to reduce curvature within the subsonic diffuser or decrease the slopes of the cowl exterior to reduce cowl wave drag. An equivalent conical angle ($\theta_{eqSD}$) can be computed for the subsonic diffuser using the length and areas at station SD and 2.

The shaping of the surfaces of the subsonic diffuser also provides some design factors. Typically, the change in slope of the surfaces is limited to avoid localized pressure gradients that could cause boundary layer separation. The distribution of area along the length of the subsonic diffuser can be tailored. One attractive approach is to set the area distribution to achieve a linear Mach number distribution. This results in a slower rate of diffusion at the start of the subsonic diffuser where the subsonic Mach numbers are higher than at the end of the subsonic diffuser.

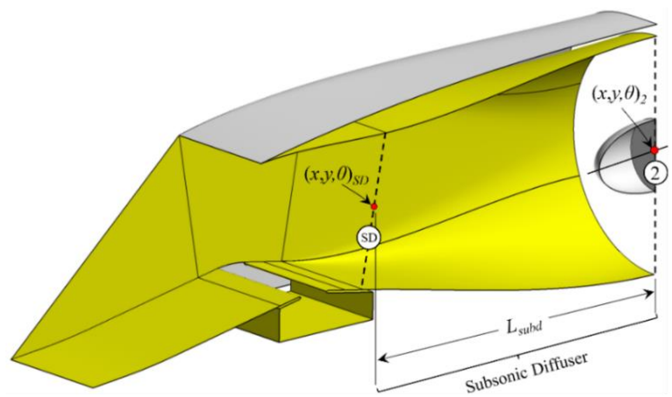


**Figure 6. Model of the subsonic diffuser of a two-dimensional inlet.**

### G. Supersonic Inlet Design and Analysis Tool (SUPIN)

The design of the inlets of this study was facilitated by using the Supersonic Inlet Design and Analysis Tool (SUPIN) [9]. SUPIN is a FORTRAN 95 program that reads in a text-based input data file that provides the values of the design factors. SUPIN uses analytic, empirical, and computational methods to design the inlet and estimate the flow rates, total pressure recovery, and drag for the inlet. SUPIN generates the surfaces of the inlet and creates a Plot3D file [12] of the surface grid of the inlet. SUPIN can also automatically generate a multi-block, structured grid for a flow domain about the inlet for flow analysis using methods of computational fluid dynamics (CFD). SUPIN is available to US persons through the NASA Software Catalog (software.nasa.gov).

## III. CFD Simulation Methods

The CFD simulations of the inlet flowfields were performed using the Wind-US flow solver, which is discussed in the next sub-section. Subsequent sub-sections discuss the modeling of the flow domain and boundary conditions for the two-dimensional, external-compression inlets, generation of the grid, flowfield initialization, and monitoring of the flow solution for iterative convergence.

### A. Wind-US Flow Solver

Wind-US [13] was used to solve the steady-state, Reynolds-averaged Navier-Stokes (RANS) equations for the flow properties at the grid points of a multi-block, structured grid defining a flow domain about the inlets. Wind-US used a cell-vertex, finite-volume representation for which the flow solution was located at the grid points and a finite-volume cell was formulated about the grid point. In Wind-US, the RANS equations were solved for the steady-state using an implicit time-marching algorithm with a first-order, implicit Euler method. Local time-stepping accelerated the convergence of the steady-state solution from an initial flow solution. All the simulations were performed assuming calorically perfect air. The inviscid fluxes of the RANS equations were modeled using a second-order, upwind Roe flux-difference splitting method. The flow simulations assumed fully turbulent flow in which the turbulent eddy viscosity was calculated using the two-equation Menter Shear-Stress Transport (SST) [14] turbulence model.

### B. Computational Flow Domain and Boundary Conditions

The computational flow domain and boundary conditions (BC) used for the CFD simulations are represented by the image of Fig. 7 for the two-dimensional inlets without a bleed slot. The flow domain defined the control volume in which the RANS equations were solved. The flow domain only contained the starboard half of the inlet since the inlet had geometric symmetry about the vertical plane through the center of the inlet and flow symmetry was assumed. Symmetry boundary conditions were imposed at the geometric symmetry boundary. The internal and external surfaces of the inlet formed a portion of the boundary of the flow domain where non-slip, adiabatic viscous wall boundary conditions were imposed. The inflow and farfield boundaries of the flow domain had freestream boundary conditions imposed in which the Mach number, pressure, temperature, and angle-of-attack were specified. The inflow and farfield boundaries were positioned just upstream of the leading-edge oblique shock wave so that the uniform freestream conditions could be imposed on those boundaries. At the downstream end of the cowl exterior, the domain had an external outflow boundary where an extrapolation boundary condition was applied for supersonic outflow. The flow domains for the simulations of the other types of inlets are similar with slight changes and are not shown here. The flow domain for the axisymmetric spike inlet contains a singular axis upstream of the nose point.

Downstream of the engine face, a converging-diverging, outflow nozzle section was added to the flow domain to set the flow rate through the engine face. The nozzle section moved the internal outflow boundary condition downstream of the engine face, which reduced possible interference from the boundary condition on the flow at the engine face. The outflow nozzle is shown in Fig. 7. The converging-diverging segment is preceded by a constant-area segment. The length of the outflow nozzle section was twice the diameter of the engine face, which was found sufficient for the inlets of this study. The cross-sectional area of the throat was set by specifying the ratio of the diameter of the nozzle throat to the diameter of the engine-face ($D_{noz}/D_2$) and was set to form choked flow at the throat. Upstream of the nozzle throat and into the subsonic diffuser, the flow was subsonic and created the necessary backpressure to support the terminal shock at the throat section. Reducing the outflow nozzle throat area increased the backpressure, and so, reduced the inlet flow rate. Downstream of the outflow nozzle throat, the flow was supersonic, and so, an extrapolation boundary condition could be applied at the internal outflow boundary. The outflow nozzle section was found to create a nearly constant corrected flow rate at the engine face. This simplified the matching of the design engine-face corrected flow rate for the inlets.

When the inlet included a bleed slot, the flow domain was extended to include the slot bleed plenum. At the downstream wall of the plenum, an outflow boundary condition was specified to extract the bleed flow from the plenum. For this, a static pressure boundary condition was imposed.

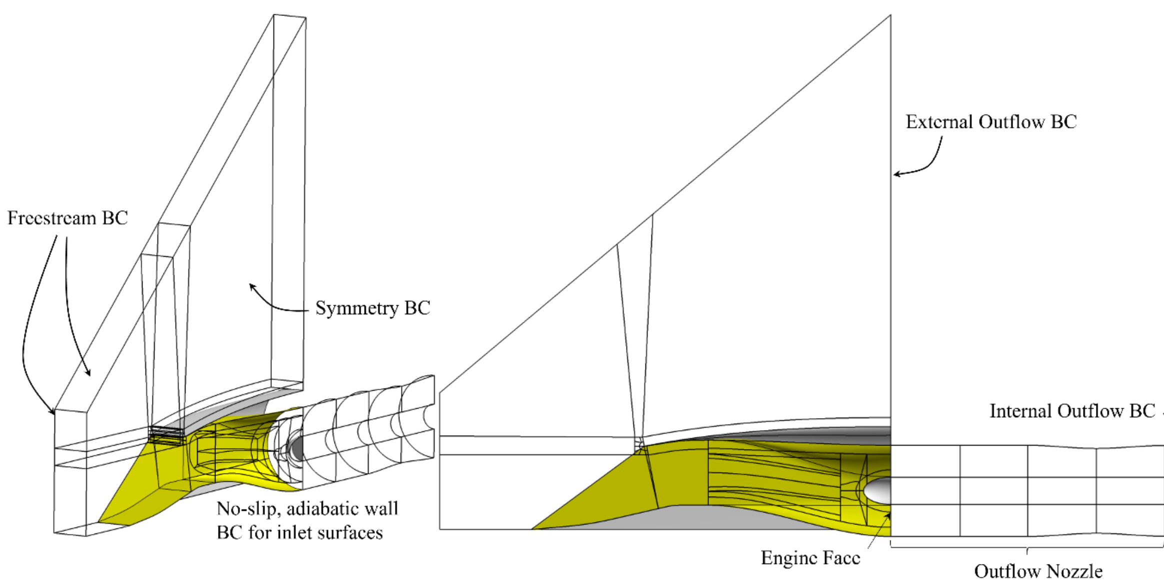


**Figure 7. Flow domain and boundary conditions for a two-dimensional inlet CFD simulations.**

### C. Computational Grid

The computational grid for the flow domain was generated by dividing the flow domain into multiple blocks and generating structured grids for each block. SUPIN was used to generate the blocks and grid points using an automated process. SUPIN also created the boundary condition file for Wind-US. The inputs to the process include some factors to determine the extents of the flow domain and the resolution of the grid points. The grid resolution factors include the grid resolution of the first grid point away from the wall ($\Delta s_{wall}$), the grid resolution within the throat section in the streamwise direction ($\Delta s_{thrt}$), and the grid resolution at the symmetry boundary ($\Delta s_{sym}$). SUPIN then imposed these grid resolution values along the edges of the inlet geometry and flow domain to compute the required number of grid points along those edges. A grid block topology was assumed for the inlet to form the edges into faces and those faces into blocks. SUPIN then generated the grids along the edges, on the surfaces, and within the interior volume of each block. The interior block boundaries abutted with other block boundaries. For most blocks, the grid lines matched across block boundaries, but some non-matched boundaries were used to facilitate the structured topology. Figure 7 shows an example of the flow domain with the multi-block topology. Figure 8 shows an example for the two-dimensional inlets of the grid lines for the block faces on the symmetry boundary. The red, blue, and green colors indicate individual faces of blocks.

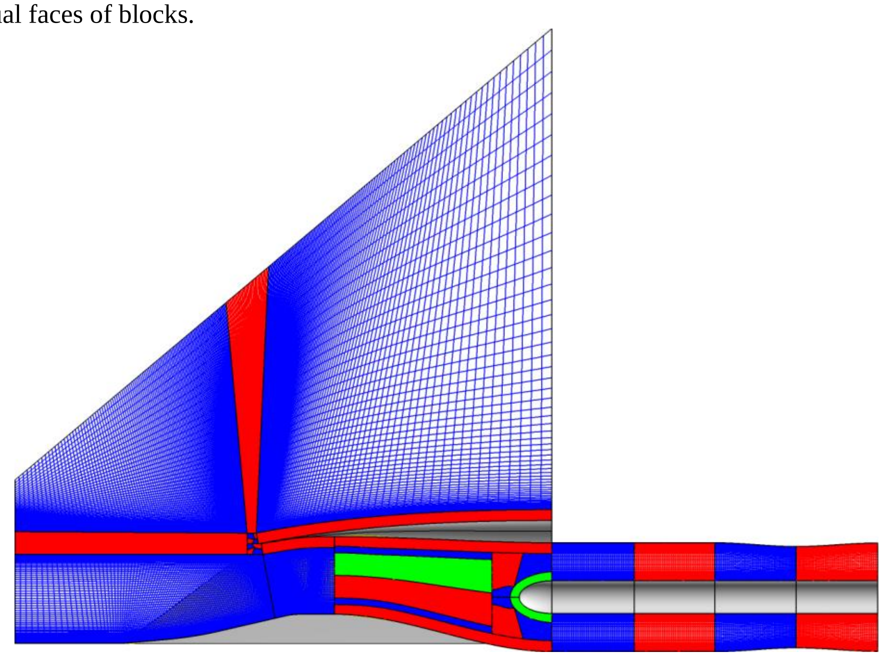

**Figure 8. Structured, multi-block, computational grids on the symmetry plane for a two-dimensional inlet.**

### D. Initial Flow Solution and Solution Monitoring

The CFD simulations were mostly initialized with a flowfield set to the freestream conditions. However, low-subsonic initial flow conditions were imposed within the bleed slot plenum. The simulation started with the first-order form of the Roe flux-splitting method to damp out large initial gradients. Eventually, the second-order flux method was applied as the residuals over the iterations decreased and the boundary layers, shock waves, and subsonic inlet flow took form. At the start of the simulations, the Courant-Friedrichs-Lewy (CFL) number had a value of 0.5 but increased incrementally to a value of 2.5 as the flow solution developed. Local time stepping was used in which the local time step used was computed based on the CFL number and the local grid cell size. The iterative convergence was indicated in part by the reduction of the root-mean-square of the residuals of the conservative variables for each block. Iterative convergence was also evaluated through the monitoring of the convergence of the inlet flow rate, total pressure recovery, and total pressure distortion. The steady-state solution was considered converged when these values changed by less than 0.001 over 1000-2000 iterations.

### E. Inlet Performance Metrics

The flow solutions from the CFD simulations were used to obtain the aerodynamic performance metrics of the inlet. The six inlet performance metrics used to characterize the inlet included the inlet flow ratio ($W_2/W_{cap}$), the inlet total pressure recovery ($p_{t2}/p_{t0}$), the inlet circumferential distortion index (DPC/P), inlet radial distortion index (DPR/P), cowl wave drag ($C_{Dwave}$), and the total surface area of the inlet normalized by the engine-face area ($S_{inlet}/A_2$).

The first metric of inlet performance was the inlet flow ratio, which was defined as the rate of mass flow passing through the engine face divided by the reference capture flow rate ($W_2/W_{cap}$). The engine-face flow rate ($W_2$) was computed from a CFD simulation as the mass-average of the flow through each of the axial grid surfaces through the outflow nozzle. The bleed flow rate ($W_{bleed}/W_{cap}$) and inlet spillage flow rate ($W_{spillage}/W_{cap}$) are related metrics.

The second metric of inlet performance was the inlet total pressure recovery, which was calculated as the mass-averaged total pressure at the engine face divided by the freestream total pressure ($p_{t2}/p_{t0}$).

The third and fourth metrics of inlet performance were descriptors of the inlet circumferential (DPC/P) and radial (DPR/P) total pressure distortion at the engine face. The distortion indices were defined on a standard 40-probe rake array and methods as defined by the Society of Automotive Engineers (SAE) Aerospace Recommended Practices (ARP) 1420 document [15]. The virtual rake array used in this study consisted of eight radial rakes each containing five total pressure probes. In the circumferential direction the eight rakes were equally spaced with 45-degree of spacing. The five probes of each rake were spaced to form five rings about the circumference of the engine face. The eight probes of each ring were located at a radius at the centroid of equal-area sectors. The flowfield from the CFD simulation was interpolated onto the locations of the probes to obtain the total pressure at the probe location. The DPC/P indices reported in this paper were computed as the average of the DPC/P indices computed on the two inner or outer rings depending on which set of rings had the higher values of circumferential distortion. The choice of the inner or outer rings establishes whether the distortion is hub or tip distortion, respectively.

The fifth metric of inlet performance is the cowl exterior wave drag coefficient ($C_{Dwave}$). The cowl exterior wave drag is the axial component of the forces due to the static pressure acting on the cowl exterior. The cowl wave drag for an inlet was computed by integrating the pressures on the cowl exterior and defining the wave drag as the axial component of the resulting pressure force vector. The value of $C_{Dwave}$ is this axial force normalized by the product of the inlet capture area ($A_{cap}$) and the freestream dynamic pressure. In general, $C_{Dwave}$ increases as the cowl lip exterior angle ($\theta_{clex}$) and forward-facing area of the cowl exterior ($S_{cwexx}$) increases.

The sixth metric of inlet performance was the total surface area of the inlet normalized by the engine-face area ($S_{inlet}/A_2$). This metric was a surrogate for the size and weight of the inlet with the assumption that $S_{inlet}$ increases as the lengths, diameters, and areas of the inlet increases, and the inlet would involve more structure that would increase its weight.

All these metrics are important to the inlet design and analysis and the choice of an optimum inlet requires a compromise in the combination of these performance metrics. For an optimum inlet, a higher total pressure recovery, lower cowl exterior wave drag coefficient, and lower distortion are considered desirable. In addition, a smaller inlet is desirable because length and surface area of the inlet can be correlated to weight. A higher weight inlet will require greater lift and thrust from the aircraft.

One approach for representing the relative effect of these performance metrics is to relate changes in the values of these metrics to change in range of the aircraft. Such a study was conducted as part of the American supersonic transport (SST) project of the late 1960s and early 1970s [16]. That aircraft was intended for Mach 2.7 cruise with a mixed-compression inlet providing airflow to an afterburning turbojet engine. The aircraft was expected to have a nominal range of 3900 miles. The expected changes in range due to the changes in the total pressure recovery, wave drag, bleed required, and weight of the inlet are listed in Table 2. It is valid to question whether these data apply to a Mach 1.4, 1.7, or 2.0 aircraft using an external-compression inlet providing airflow to a non-afterburning turbofan engine. Certainly, an updated study of the effect of these inlet performance metrics is warranted. However, it is felt that the data of Table 2 provides a relative effect of the performance metrics and can be useful for the optimization of the inlets of this study. The change in the metrics is with respect to a reference inlet and here we consider reference values from the modeling and simulation of the Mach 1.7 Gulfstream / NASA Low-Boom Single-Stream (LBSS) inlet [17]. Reference values of the performance metrics were obtained from the modeling of the LBSS inlet within SUPIN and CFD simulations and are listed in Table 2. A surrogate for the weight of the inlet is provided by the surface area of the inlet normalized by the annular area of the engine face ($S_{inlet}/A_2$).

**Table 2. Effect of inlet performance metrics on aircraft range.**

| | $p_{t2}/p_{t0}$ | $C_{Dwave}$ | $W_{bleed}/W_{cap}$ | ***Weight*** |
|---|---|---|---|---|
| Metric Δ | -0.01 | 0.01 | 0.01 | 0.10 |
| Range Δ | -32 | -41 | -23 | -17 |
| LBSS | 0.9470 | 0.0930 | 0.0 | 16.64 |

The overall aircraft range increment ($\Delta R$) is expressed as a sum of change in range increments due to the four performance metrics listed in Table 2,

$$\Delta R = \Delta R_R + \Delta R_D + \Delta R_B + \Delta R_W \tag{1}$$

where $\Delta R_R$, $\Delta R_D$, $\Delta R_B$, and $\Delta R_W$, are the range increments due to the inlet total pressure recovery, wave drag, bleed, and weight, respectively. A larger value of $\Delta R$ indicated a better inlet. There increments are calculated as,

$$\Delta R_R = \left[\frac{p_{t2}}{p_{t0}} - \left(\frac{p_{t2}}{p_{t0}}\right)_{Ref}\right]\left(\frac{-32}{-0.01}\right) \tag{2}$$

$$\Delta R_D = \left[\, C_{Dwave} - (C_{Dwave})_{Ref}\,\right]\left(\frac{-41}{0.01}\right) \tag{3}$$

$$\Delta R_B = \left[\frac{W_{bleed}}{W_{cap}} - \left(\frac{W_{bleed}}{W_{cap}}\right)_{Ref}\right]\left(\frac{-23}{0.01}\right) \tag{4}$$

and

$$\Delta R_W = \left[\frac{\frac{S_{inlet}}{A_2} - \left(\frac{S_{inlet}}{A_2}\right)_{Ref}}{\left(\frac{S_{inlet}}{A_2}\right)_{Ref}}\right]\left(\frac{-17}{0.10}\right) \tag{5}$$

## IV. Results

The design process was applied for each of the five types of inlets and at the freestream Mach numbers of $M_0$ = 1.4, 1.7, and 2.0 to create 15 inlets. Two flattop streamline-traced inlets were also created as part of the study. The first subsection summarizes the design factors and geometric characteristics of the inlets. Subsequent subsections provide further details for some of the inlet types and presents some images from the CFD simulations. Subsections then present the inlet aerodynamic performance for the on-design and off-design conditions.

### A. Summary of the Inlet Designs

Images of the inlets are presented in Fig. 9 as side-views of the inlets cut at the vertical plane-of-symmetry at $z$ = 0.0 for the five inlet types and three Mach numbers. The images of Fig. 9 were scaled to reflect the same engine-face diameters ($D_2$) of the inlets. Thus, the images provide a comparison of the overall sizes of the inlets. Not shown in Fig. 9 are the two flattop streamline-traced inlets. Each of the inlets were the result of several iterations of the inlet design for a particular freestream Mach number and inlet type and represent the "best" inlet designed as part of this study. In the case of the axisymmetric spike inlets, formal design-of-experiments (DOE) methods and response surface methods (RSM) were applied to refine those inlets [8].

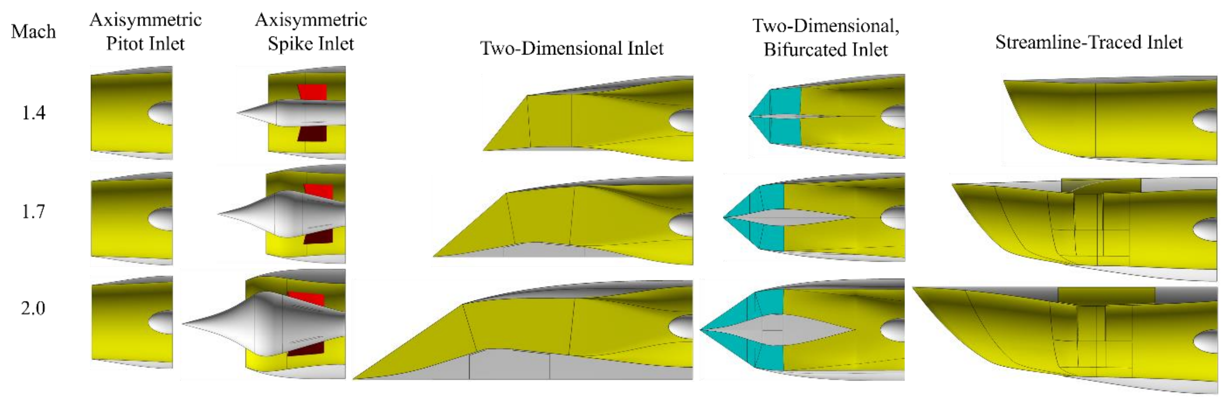


**Figure 9. Images of the fifteen inlets for the freestream Mach numbers and inlet types.**

Table 3 lists some of the design factors and physical dimensions of the inlets. The labels "2D Bif" and "ST" are the abbreviation for the two-dimensional, bifurcated and streamline-traced inlets, respectively. All the lengths and areas listed in Table 3 were normalized by the engine-face diameter ($D_2$) and area ($A_2$), respectively.

The surface area of the external supersonic diffuser ($S_{comp}$) provides a measure of the size of the external supersonic diffuser. Table 3 lists the surface area of the cowl exterior that projects into the axial direction ($S_{cwexx}$), which provides a sense of the cowl wave drag that can be expected for the inlet. A larger axial area usually results in a larger cowl wave drag. The total surface area of the inlet ($S_{inlet}$) provides a sense of the overall size of the inlet, which may be correlated to the weight of the inlet.

The design of the inlets involves a sizing iteration in which the total pressure losses through the inlet are estimated and the capture area ($A_{cap}$) is adjusted until the inlet captures the amount of airflow desired by the engine at the design conditions. Table 3 lists the capture area for each inlet normalized by the engine-face area ($A_{cap}$ / $A_2$).

**Table 3. Design factors and physical dimensions of the inlets.**

| $M_0$ | Type | $N_{stgs}$ | $M_{EX}$ | $\theta_{clin}$ | $M_1$ | $L_{thrt}/D_2$ | $L_{subd}/D_2$ | $L_{inlet}/D_2$ | $S_{comp}/A_2$ | $S_{cwexx}/A_2$ | $S_{inlet}/A_2$ | $A_{cap}/A_2$ |
|---|---|---|---|---|---|---|---|---|---|---|---|---|
| 1.4 | Axi-Pitot | - | 1.40 | 3.0 | 0.74 | 0.0 | 1.0 | 1.0 | 0.0 | 0.287 | 6.105 | 0.948 |
| | Axi-Spike | 1 | 1.28 | 4.0 | 0.79 | 0.154 | 0.5 | 1.11 | 0.309 | 0.260 | 7.250 | 0.974 |
| | 2D | 1 | 1.25 | 2.0 | 0.81 | 0.523 | 1.5 | 2.59 | 1.364 | 0.453 | 18.36 | 0.953 |
| | 2D-Bif | 1 | 1.25 | 2.0 | 0.81 | 0.370 | 1.3 | 1.95 | 1.072 | 1.185 | 19.81 | 0.937 |
| | ST Round | 1 | 1.18 | -5.0 | 0.90 | 0.314 | 1.5 | 2.64 | 3.376 | 0.373 | 20.25 | 0.972 |
| 1.7 | Axi-Pitot | - | 1.70 | 3.0 | 0.64 | 0.0 | 1.0 | 1.0 | 0.0 | 0.292 | 6.097 | 0.943 |
| | Axi-Spike | 3 | 1.38 | 8.1 | 0.79 | 0.254 | 0.8 | 1.737 | 0.711 | 0.370 | 14.57 | 1.061 |
| | 2D | 3 | 1.35 | 6.0 | 0.76 | 0.766 | 1.5 | 3.233 | 2.413 | 0.481 | 22.47 | 1.107 |
| | 2D-Bif | 3 | 1.30 | 9.0 | 0.79 | 0.281 | 1.5 | 2.258 | 1.908 | 1.169 | 23.66 | 1.086 |
| | ST Round | 1 | 1.27 | -5.0 | 0.90 | 0.483 | 1.5 | 3.325 | 5.485 | 0.406 | 26.37 | 1.118 |
| | ST Flattop | 1 | 1.27 | -5.0 | 0.90 | 0.403 | 2.0 | 3.587 | 5.340 | 0.568 | 30.96 | 1.118 |
| 2.0 | Axi-Pitot | - | 2.00 | 3.0 | 0.58 | 0.0 | 1.0 | 1.0 | 0.0 | 0.311 | 6.069 | 0.924 |
| | Axi-Spike | 3 | 1.38 | 17.0 | 0.75 | 0.288 | 1.0 | 2.160 | 1.248 | 0.412 | 15.65 | 1.221 |
| | 2D | 3 | 1.40 | 12.0 | 0.74 | 1.270 | 1.5 | 4.192 | 3.742 | 0.613 | 31.33 | 1.299 |
| | 2D-Bif | 3 | 1.40 | 12.6 | 0.74 | 0.309 | 1.5 | 2.536 | 2.895 | 1.690 | 26.32 | 1.299 |
| | ST Round | 1 | 1.37 | -5.0 | 0.90 | 0.431 | 1.5 | 3.775 | 6.905 | 0.597 | 29.55 | 1.331 |
| | ST Flattop | 1 | 1.37 | -5.0 | 0.90 | 0.330 | 2.0 | 3.952 | 6.725 | 0.311 | 33.88 | 1.331 |

A subset of the data of Tables 3 are plotted and presented in Fig. 10. The variation of the capture areas normalized by the engine face area with respect to the freestream Mach number is plotted in the set of plots of the left-hand-side of Fig. 10. The lengths of the inlet are plotted in the middle set of plots of Fig. 10. The general trend is that the capture area and lengths increase with increasing Mach number with a nearly linear variation. The exception are the axisymmetric pitot inlets, which stay much the same. These variations can be seen in the images of the inlets of Fig. 9. The longest inlets are the two-dimensional and streamline-traced inlets, which are roughly the same length, but are almost twice as long as the axisymmetric spike inlets. The two-dimensional, bifurcated inlet does provide a means of retaining the two-dimensional character of the inlet while resulting in a shorter inlet.

The plots of the right-hand-side of Fig. 10 show the variations of the total surface area of the inlets, which includes the surfaces of the external supersonic diffuser, throat section, subsonic diffuser, and cowl exterior. A greater total surface area may correlate with a greater weight for the inlet. As with the lengths of the inlets, the two-dimensional and streamline-traced inlets are the inlets with the greatest total surface area.

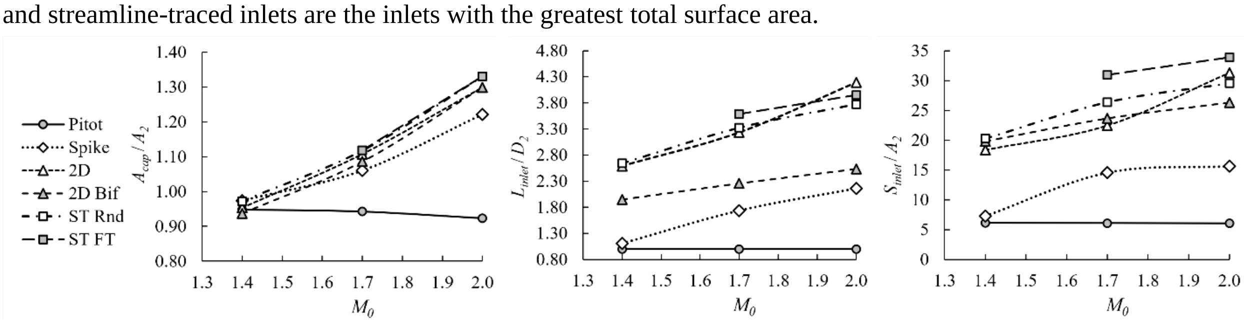


**Figure 10. Variation of the capture areas, lengths, and surface area of the inlets with respect to the freestream Mach number.**

## B. Axisymmetric Spike Inlets

The axisymmetric spike inlets of this study are the same as those presented in Ref. [8]. The refinement of those inlets involved using design-of-experiments (DOE) and response-surface modeling (RSM) to arrive at optimum values for $M_{EX}$, throat section shoulder radius, and subsonic diffuser length ($L_{subd}$) to maximize the range increment as described in Section III.E above.

The axisymmetric spike inlet for $M_0$ = 1.4 featured a single-stage cone of 15.15 degrees for the external supersonic diffuser that decelerated the flow to $M_{EX}$ = 1.2825. The external supersonic diffuser smoothly mated to a cylindrical centerbody equal to the diameter of the spinner hub. The cowl lip angle was $\theta_{clip}$ = 4.0 degrees, which was slightly higher than the local flow angle of 2.56 degrees. This offset allowed a smooth cowl interior from the cowl lip to the tip of the engine face. The cowl exterior angle was $\theta_{clex}$ = 7.0 degrees, which resulted in a continuously smooth cowl exterior. Images of the inlet can be seen in Fig. 11 along with Mach number contours on the symmetry plane and at axial stations from the CFD simulation at the critical flow condition. The leading conical shock wave intersects the cowl lip and the terminal shock wave is normal about the annular entrance at station 1. Subsonic flow is diffused within the interior ducting with a small and well-behave boundary layer.

The axisymmetric spike inlet for $M_0$ = 1.7 featured a three-stage external supersonic diffuser that decelerated the flow to $M_{EX}$ = 1.38. Images of the inlet can be seen in Fig. 12 along with Mach number contours on the symmetry plane and at axial stations from the CFD simulation at the critical flow condition. The second stage creates Mach waves for isentropic compression. The cowl lip angle was specified to be aligned with the local flow, and so $\theta_{clip}$ = 8.1 degrees. The cowl lip exterior angle was set to $\theta_{clex}$ = 13.1 degrees. The throat section was designed to gradually turn the flow toward the engine face using a circular arc for the centerbody. The Mach number contours show the normal terminal shock wave placed at the inlet entrance at station 1. The Mach number contours show the boundary layers thickening through the terminal shock wave interaction and inlet interior. The inlet contains four support struts that secure the centerbody with the cowling. The Mach contour at the engine face show the disturbance in the flow at the wake from the end of the support struts.

The axisymmetric spike inlet for $M_0$ = 2.0 also used a normal terminal shock wave. Attempts were made to obtain a strong oblique terminal shock wave with a shoulder bleed region. This allowed a higher of $M_{EX}$ which was intended to reduce the cowl lip angle, and so reduce cowl wave drag. However, the attempts were not successful. This could be because along the terminal shock wave, the Mach number is lower at the centerbody than the cowl lip.

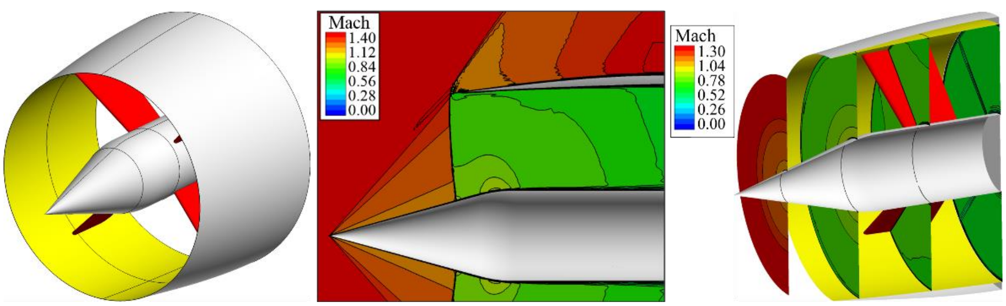


**Figure 11. The axisymmetric spike inlet for $M_0$ = 1.4.**

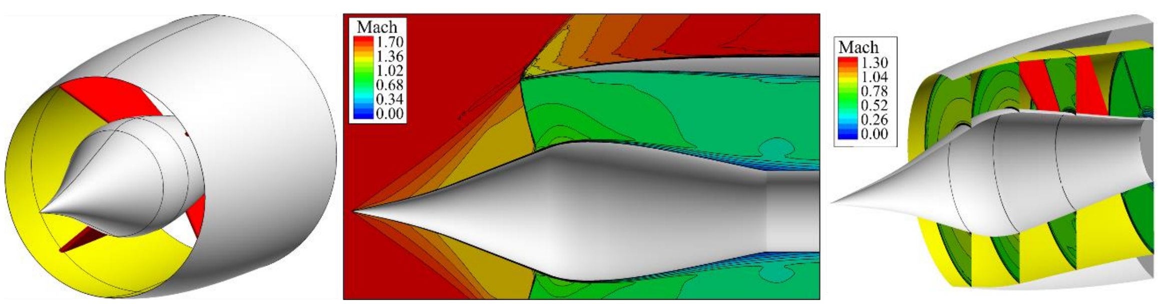


**Figure 12. The axisymmetric spike inlet for $M_0$ = 1.7.**

### C. Two-Dimensional Inlets

The lessons of Refs. [2] and [6] were applied to the design of the two-dimensional inlets. The external supersonic diffuser for the inlet for $M_0$ = 1.4 had only a single-stage ramp while the inlets for $M_0$ = 1.7 and 2.0 had three stages with the second stage being a curved isentropic section. The inlet for $M_0$ = 2.0 used a strong oblique shock wave much in the manner of the inlet for the Concorde aircraft [6]. The cowl lip interior angles, $\theta_{clin}$, were set to be at or slightly below the local flow angle at the cowl lip. The throat sections were specified to turn the flow back toward the engine face but involved a gradually increasing cross-sectional area through the throat section.

The inlet for $M_0$ = 2.0 is shown on the left of Fig. 13. A bleed slot was used to create a strong oblique terminal shock wave with $M_{EX}$ = 1.40. The upper image on the right-hand-side of Fig. 13 shows the Mach contours on the symmetry plane and show that at the critical operating condition, a strong oblique terminal shock wave is formed at the entrance station 1. The inlet yielded good performance, which is summarized in the last subsection. A feature of two-dimensional inlets is the formation of a vortex in the lower corners. The vortex seems to originate by the deflection downward of the flow on the sidewall downstream of the terminal shock wave. This downward flow forms the vortex when the flow reaches the lower ramp surfaces. The bleed slot helps to reduce the adverse effects of this vortex. As the vortex propagates downstream, it is diffused somewhat by the subsonic diffuser.

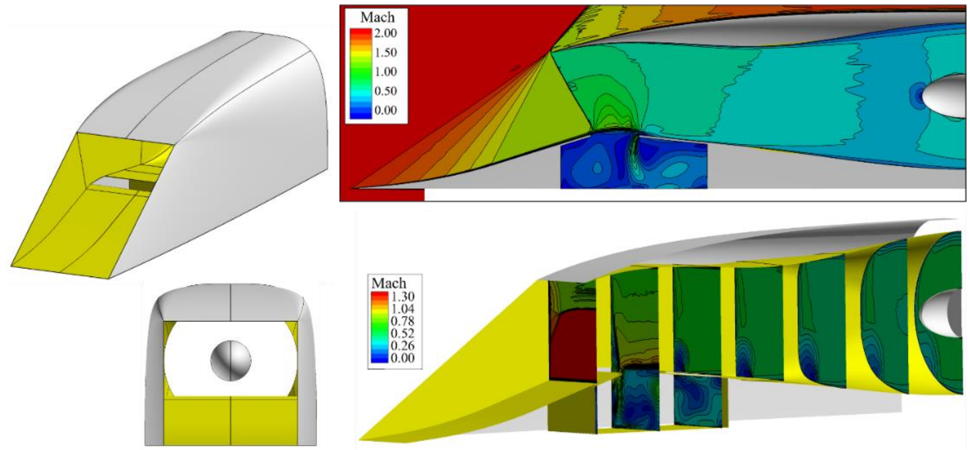


**Figure 13. The two-dimensional inlet for $M_0$ = 2.0.**

### D. Two-Dimensional, Bifurcated Inlets

The two-dimensional bifurcated inlets are formed by mirroring two-dimensional inlets about the horizontal plane through the inlet axis. Each half has its own external supersonic diffuser and throat sections. Within SUPIN, the two-dimensional, bifurcated inlets are designed using the same methods as the two-dimensional inlets, except the sizing is performed using half of the engine face as for the two-dimensional inlets. In modeling the subsonic diffuser, the centerbody ends before the start of the spinner so that both halves of the inlet have a common mixing region ahead of the engine face. Images of the two-dimensional, bifurcated inlet for $M_0$ = 2.0 are shown in Fig. 14. As discussed previously, the two-dimensional, bifurcated inlet provides a means of having a two-dimensional inlet while reducing the length as compared to the regular two-dimensional inlet. The bottom image of Fig. 14 shows Mach number contours on the symmetry plane for the critical operating condition. The strong oblique terminal shock wave interacts with the bleed slot. Most of the bleed flow into the slot is concentrated in a supersonic jet at the back of the slot. Such feature was noted in the Concorde inlet [6].

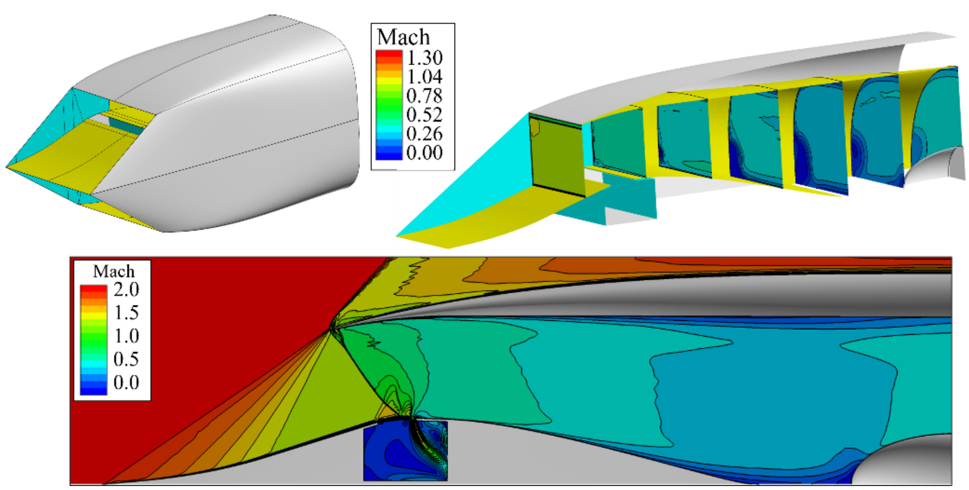


**Figure 14. The two-dimensional, bifurcated inlet for $M_0$ = 2.0.**

### E. Streamline-Traced Inlets

The streamline-traced inlets used an axisymmetric, inward-turning parent flowfield to form the external supersonic diffuser through streamline tracing. Various shapes of the inlets are possible based on the choice of the tracing cross-section used. Streamline-traced inlets were designed for $M_0$ = 1.4, 1.7, and 2.0 using circular and flattop tracing cross-sections similar to those described in Ref. [5]. The flattop tracing cross-section flattens the top portion of the capture cross-section and could integrate better with a wing or fuselage than a round capture cross-section. Images of the round and flattop streamline-traced inlet for $M_0$ = 2 are shown in Figs. 15 and 16, respectively. The inlets feature a scarfed leading edge due to an offset of the tracing curve above the axis-of-symmetry. This provides a cut-out for spillage of subsonic flow at the downstream portion of the leading edge. The inlets contain a bleed slot at the shoulder of the inlet.

The images on the right-hand-sides in Figs. 15 and 16 show Mach number contours on the symmetry plane and at axial stations. The leading-edge shock and Mach waves are illustrated in the Mach contours. The terminal shock wave wraps about the cowl lip at the bottom of the inlet and projects downstream into the inlet. The angle of the terminal shock wave indicates that it is a strong oblique shock wave. The terminal shock wave interacts with the bleed slot and forms a small supersonic region that terminates with a small normal shock wave at the end of the bleed slot. This shock wave structure is the same as observed with the Concorde inlet [6] and previous streamline-traced inlet studies [5]. The Mach number contours along the axial stations show a region of low-momentum flow at the top of the subsonic diffuser that propagates to the engine face. This low-momentum region was present in earlier studies [4,5] for streamline-traced inlets and is due to adverse interactions of the terminal shock with the thick boundary layer at the top-center of the inlet.

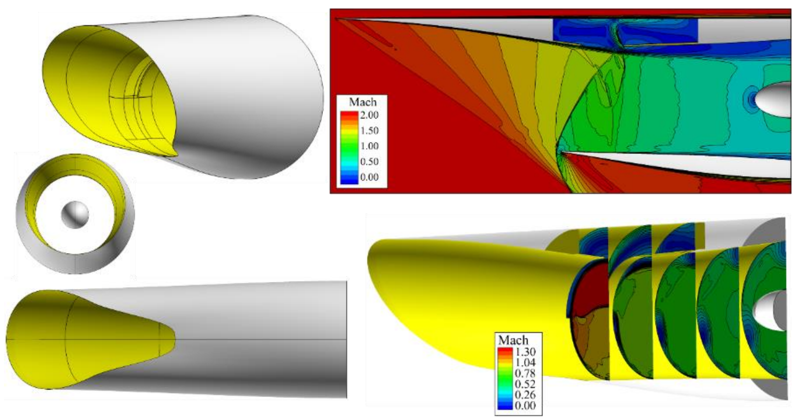


**Figure 15. The round streamline-traced inlet for $M_0$ = 2.0.**

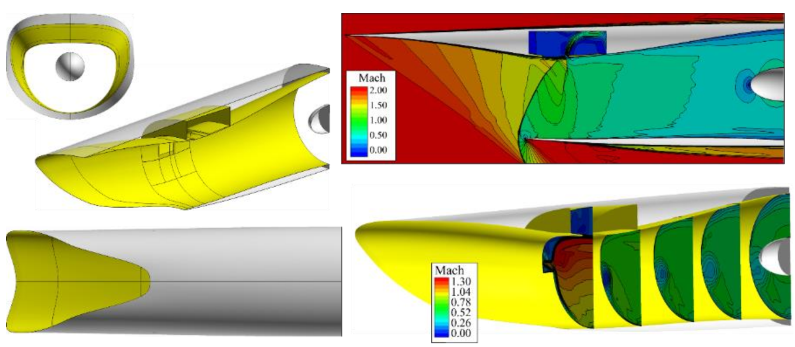


**Figure 16. The flattop streamline-traced inlet for $M_0$ = 2.0.**

### F. Aerodynamic Performance of the Inlets for the On-Design, Critical Operating Conditions

The on-design aerodynamic performance of the inlets is characterized by the inlet flow rates, total pressure recovery, wave drag, and total pressure distortion with the inlet operating at its freestream Mach number ($M_0$) and critical condition in which the engine face is at its specified corrected flow rate ($W_{C2}$) as listed in Table 1. The inlet aerodynamic performance metrics are listed in Table 4. The estimates of the performance metrics obtained from SUPIN can be compared to those from CFD simulations.

All the inlets were designed for zero subsonic and supersonic spillage; however, some level of spillage was observed from the CFD simulations with the streamline-traced inlets showing the greatest level of spillage. The two-dimensional and streamline-traced inlets were designed with bleed slots and 3% and 5% bleed for $M_0$ = 1.7 and 2.0, respectively.

A subset of the data in Table 4 for the CFD simulations are plotted in Figs. 17 and 18. The plots of the total pressure recoveries on the left-hand-side of Fig. 17 suggests that similar recovery can be obtained from either the axisymmetric spike, two-dimensional, or streamline-traced inlets, especially at $M_0$ = 1.7 and 2.0. The plots of the wave drag coefficients on the right-hand-side of Fig. 17 show that the inward-turning nature of the streamline-traced inlets results in lower wave drag coefficients. The plots of Fig. 18 show the variation of the radial and circumferential total pressure distortion indices as computed from the CFD simulations. The upper limit of DPR/P = DPC/P = 0.10 is also plotted and all indices of the inlets are below the limit. The higher distortion levels for the streamline-traced inlets were likely due to the low-momentum region that formed at the top of the subsonic diffuser of those inlets. None of the inlets employed vortex generators in the subsonic diffuser which could further reduce total pressure distortion.

**Table 4. Aerodynamic performance of the inlets for the on-design critical conditions.**

| $M_0$ | Type | SUPIN | | CFD | | | | | | |
|---|---|---|---|---|---|---|---|---|---|---|
| | | $p_{t2}/p_{t0}$ | $C_{Dwave}$ | $W_{spillage}/W_{cap}$ | $W_{bleed}/W_{cap}$ | $W_2/W_{cap}$ | $p_{t2}/p_{t0}$ | $C_{Dwave}$ | DPC/P | DPR/P |
| 1.4 | Axi Pitot | 0.9556 | 0.0538 | 0.20% | 0.0 | 0.9980 | 0.9547 | 0.0524 | 0.0 | 0.0 |
| | Axi Spike | 0.9793 | 0.0442 | 0.66% | 0.0 | 0.9934 | 0.9756 | 0.0451 | 0.0279 | 0.0088 |
| | 2D | 0.9749 | 0.1360 | 0.47% | 0.0 | 0.9953 | 0.9541 | 0.1502 | 0.0744 | 0.0876 |
| | 2D-Bif | 0.9821 | 0.1925 | 0.66% | 0.0 | 0.9934 | 0.9369 | 0.2047 | 0.0905 | 0.0501 |
| | ST Round | 0.9887 | 0.0164 | 0.99% | 0.0 | 0.9901 | 0.9709 | 0.0145 | 0.0154 | 0.0715 |
| 1.7 | Axi-Pitot | 0.8539 | 0.0428 | 0.21% | 0.0 | 0.9979 | 0.8532 | 0.0428 | 0.0 | 0.0 |
| | Axi-Spike | 0.9598 | 0.0611 | 1.08% | 0.0 | 0.9892 | 0.9526 | 0.0619 | 0.0081 | 0.0123 |
| | 2D | 0.9380 | 0.0776 | 1.09% | 3.14% | 0.9577 | 0.9611 | 0.0798 | 0.0263 | 0.0399 |
| | 2D-Bif | 0.9716 | 0.1031 | 0.55% | 1.33% | 0.9812 | 0.9656 | 0.0984 | 0.0338 | 0.0262 |
| | ST Round | 0.9812 | 0.0189 | 2.28% | 3.0% | 0.9472 | 0.9585 | 0.0358 | 0.0699 | 0.0744 |
| | ST Flattop | 0.9497 | 0.0747 | 2.63% | 2.26% | 0.9511 | 0.9640 | 0.0296 | 0.0174 | 0.0650 |
| 2.0 | Axi-Pitot | 0.7195 | 0.0406 | 0.02% | 0.0 | 0.9996 | 0.7188 | 0.0421 | 0.0 | 0.0 |
| | Axi-Spike | 0.9578 | 0.0859 | 0.93% | 0.0 | 0.9907 | 0.9440 | 0.0978 | 0.0151 | 0.0103 |
| | 2D | 0.9467 | 0.1056 | 1.24% | 5.0% | 0.9376 | 0.9484 | 0.1049 | 0.0328 | 0.0349 |
| | 2D-Bif | 0.9501 | 0.1065 | 1.04% | 4.52% | 0.9444 | 0.9555 | 0.1065 | 0.0212 | 0.0290 |
| | ST Round | 0.9686 | 0.0169 | 3.38% | 5.0% | 0.9162 | 0.9495 | 0.0187 | 0.0449 | 0.0613 |
| | ST Flattop | 0.9875 | 0.0164 | 4.00% | 4.81% | 0.9119 | 0.9477 | 0.0050 | 0.0219 | 0.0575 |

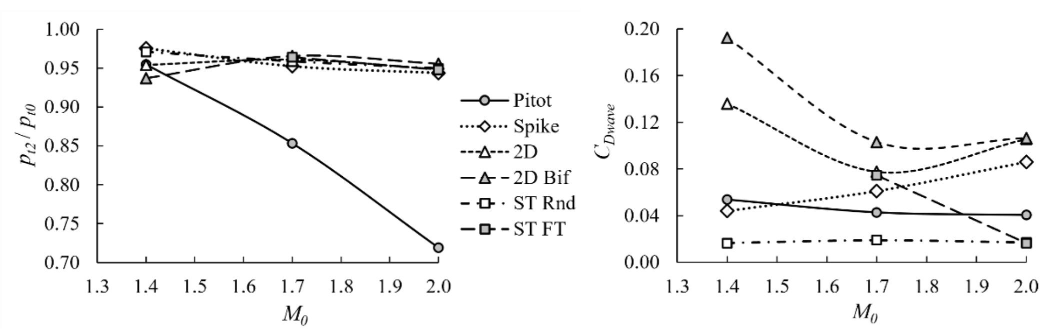


**Figure 17. Variation of the total-pressure recovery (left) and wave drag (right) for the inlets at the critical operating condition with respect to the freestream Mach number.**

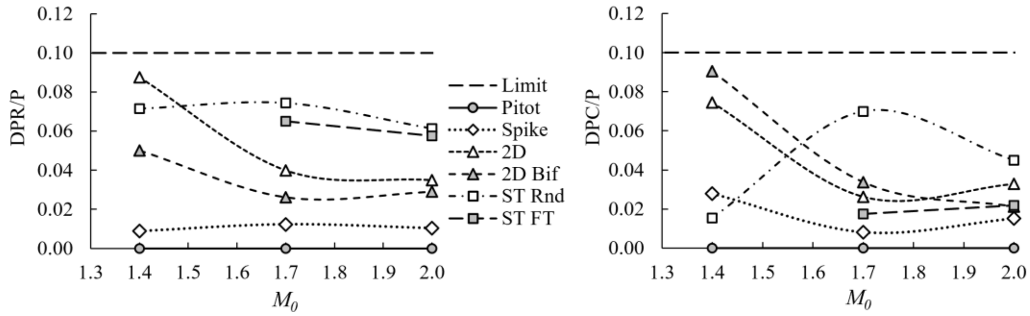


**Figure 18. Variation of the radial (left) and circumferential (right) total-pressure distortion for the inlets at the critical operating condition with respect to the freestream Mach number.**

A summary of the range increments for each of the freestream Mach number and inlet types is presented in Table 5. The data provides a useful insight on the relative effects of each of the performance metrics on the expected range of an aircraft. The focus should be on the values of the range increments relative to the others rather than on the absolute value of the range increments. The higher values of $\Delta R$ indicate a better value of the metric. For the $M_0$ = 1.4 inlets, the axisymmetric spike inlet with $\Delta R$ = 396 suggests this inlet is preferred based on the on-design, critical operating condition. The round streamline-traced inlet also looks favorable due do its low wave drag despite indicating a heavier inlet than the axisymmetric spike inlet. Even the axisymmetric pitot inlet is a contender for a simple inlet solution. The two-dimensional inlets suffer from higher cowl wave drag, which makes them not desirable.

**Table 5. Range increments of the inlets for the on-design critical conditions.**

| $M_0$ | Type | $\Delta R_R$ | $\Delta R_D$ | $\Delta R_B$ | $\Delta R_W$ | $\Delta R$ |
|---|---|---|---|---|---|---|
| 1.4 | Axi-Pitot | 25 | 166 | 0 | 108 | 299 |
| | Axi-Spike | 103 | 196 | 0 | 96 | **396** |
| | 2D | 23 | -234 | 0 | -18 | -229 |
| | 2D-Bif | -32 | -458 | 0 | -32 | -523 |
| | ST Round | 76 | 322 | 0 | -37 | 361 |
| 1.7 | Axi-Pitot | -300 | 206 | 0 | 108 | 14 |
| | Axi-Spike | 41 | 127 | 0 | 21 | **189** |
| | 2D | -29 | 54 | -72 | -60 | -106 |
| | 2D-Bif | 79 | -41 | -31 | -72 | -65 |
| | ST Round | 37 | 235 | -69 | -99 | 103 |
| | ST Flattop | 54 | 260 | -52 | -146 | 116 |
| 2.0 | Axi-Pitot | -730 | 209 | 0 | 108 | -413 |
| | Axi-Spike | -10 | -20 | 0 | 10 | -20 |
| | 2D | 5 | -49 | -115 | -150 | -309 |
| | 2D-Bif | 27 | -55 | -104 | -99 | -231 |
| | ST Round | 8 | 305 | -115 | -132 | 65 |
| | ST Flattop | 2 | 361 | -111 | -176 | **76** |

For the $M_0$ = 1.7 inlets, the axisymmetric spike inlet with $\Delta R$ = 189 suggests this inlet is preferred. The flattop streamline-traced inlet with its low wave drag also ranks well despite its larger size and weight than the axisymmetric spike inlet. The two-dimensional inlets again suffer from higher cowl wave drag than the other inlets.

For the $M_0$ = 2.0 inlets, the flattop streamline-traced inlet looks like the most favorable with $\Delta R$ = 76. The axisymmetric spike inlet suffers from increased cowl wave drag due to the higher cowl lip exterior angles. The lower cowl wave drag of the streamline-traced inlets with respect to the other inlets helps in its relative standing.

The selection of the inlet type for a specific $M_0$ depends not only on its performance at the on-design, critical operating conditions, but also on its behavior at off-design conditions. Some of this performance will be presented in the following sections. While it may be possible to reduce or eliminate the need for bleed at the on-design conditions, it may be useful maintaining performance and stability for off-design conditions.

### G. Aerodynamic Performance of the Inlets at the Design Mach Number with Variation of the Inlet Flowrate

The off-design performance of the inlets at the design $M_0$ with variation in the engine flow rate is expressed through the characteristic curves of the total pressure recovery ($p_{t2}/p_{t0}$), radial distortion (DPR/P), and circumferential distortion (DPC/P) with respect to the engine-face flow ratio ($W_2/W_{cap}$). The characteristic curves are obtained from

CFD simulations and shown in Fig. 19. The left, middle, and right column of plots are for the $M_0$ = 1.4, 1.7, and 2.0 inlets, respectively. The vertical portion of the curves indicates a constant flow ratio and is the supercritical leg of the curve. As the terminal shock wave moves forward of the cowl lip plane and spills subsonic flow or the bleed increases, the engine-face flow ratio decreases and forms the subcritical leg of the curve. The critical operating point was designed to occur with the condition of maximum total pressure recovery with maximum engine-face flow ratio.

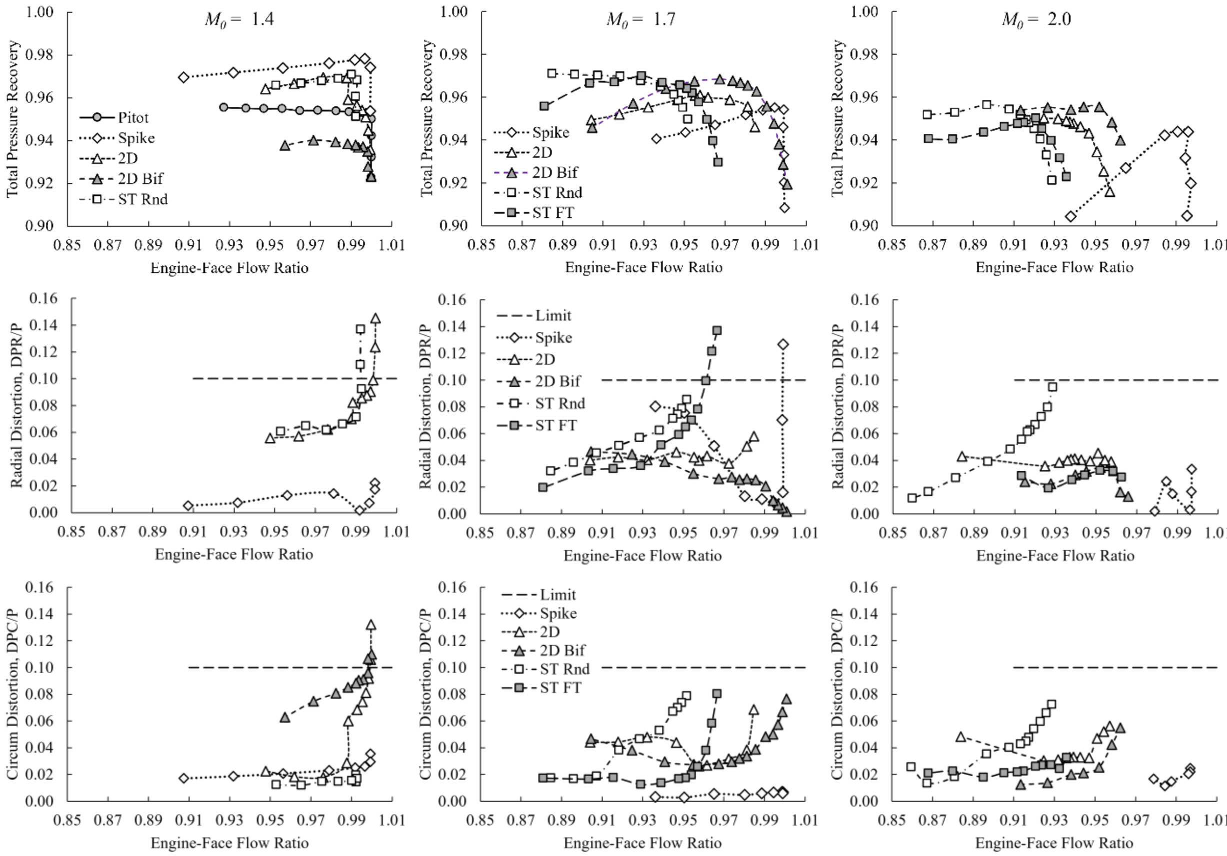


**Figure 19. Characteristic curves for the total pressure recovery, radial distortion, and circumferential distortion with respect to engine-face flow ratio for $M_0$ = 1.4, 1.7, and 2.0 (left, middle, right columns).**

The curves for the total pressure recovery for the axisymmetric spike and two-dimensional inlets show a decrease in total pressure recovery as the flow become more subcritical. This decrease is greater as $M_0$ increases. The decrease in total pressure recovery is not as severe for the streamline-traced inlets. The decrease is not desirable and likely the inlet controls would avoid the inlets for operating in that condition. Attempts at using bleed to stabilize the upstream movement of the terminal shock wave for the axisymmetric inlet at $M_0$ = 2.0 proved unsuccessful [8].

All inlets seemed to have good radial and circumferential distortion behavior below the limits through the variation in engine-face flow. The exceptions are those operating points at the extreme ends of the supercritical conditions where the terminal shock wave is well within the inlet. It is likely, the inlet and engine controls would prevent the inlet from operating at those conditions.

### H. Aerodynamic Performance of the Inlets with Variation of the Mach Number and Angle-of-Attack

The inlets were analyzed using CFD simulations for off-design conditions of angle-of-attack and increments of freestream Mach number. The variations in the inlet recovery and flow ratios can be seen in Fig. 20. For the axisymmetric spike inlets, the angle-of-attack was varied to a maximum positive angle-of-attack of $\alpha_0$ = 5 degrees. The general trend for axisymmetric spike inlets is that inlet recovery and flow ratio decrease with increased angle-of-attack. For the streamline-traced inlets at $M_0$ = 1.7 and 2.0, the angles-of-attack varied with both negative and positive angles-of-attack to a maximum values of $\alpha_0$ = ±4 degrees. The plots of Fig. 20 show a much more dramatic change in inlet recovery and flow ratio with change in angle-of-attack for the streamline-traced inlets than for the axisymmetric spike inlets. At $M_0$ = 2.0, the change in inlet recovery for the axisymmetric spike inlet was $\Delta p_{t2}/p_{t0} \approx$

0.021 while for the streamline-traced inlet it was $\Delta p_{t2}/p_{t0} \approx 0.078$. This suggests that the streamline-traced inlets are sensitive to angle-of-attack and would benefit from an integration with the wing or fuselage to shield the inlet from such changes in angle-of-attack. The variation in freestream Mach number was $\Delta M_0 = \pm 0.05$ and $\pm 0.10$.

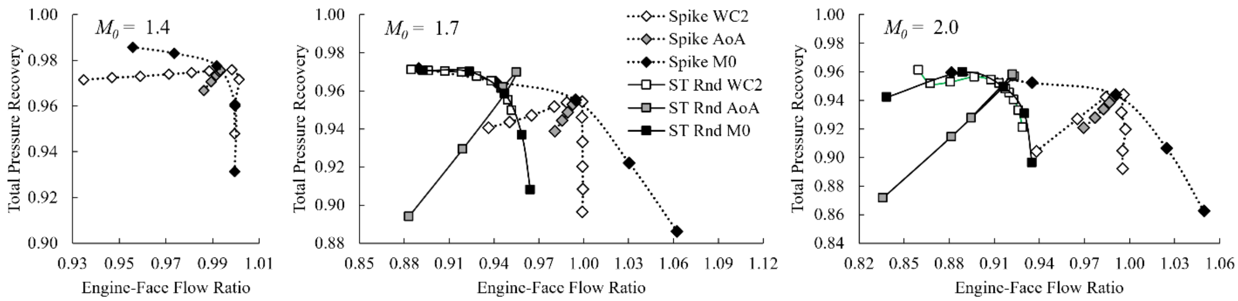


**Figure 20. Characteristic curves for the total pressure recovery for M0 = 1.4, 1.7, and 2.0 with respect to variation in engine-face corrected flow (WC2), angle-of-attack (AoA), and freestream Mach number (M0).**

## V. Conclusion

The designs of supersonic external-compression inlets were refined for the cruise conditions for the combination of three freestream Mach numbers of $M_0$ = 1.4, 1.7, and 2.0 and the five inlet types, which were the axisymmetric pitot, axisymmetric spike, two-dimensional, two-dimensional bifurcated, and streamline-traced inlets. Their physical dimensions and aerodynamic performance were discussed and compared. For each inlet, the engine-face flow ratio was varied to create the characteristic curves for the total pressure recovery and the radial and circumferential total pressure distortion indices. Off-design performance that examined angle-of-attack and Mach number variations was evaluated. Some conclusions from the study are:

- Similar levels of the total pressure recovery seem to be achievable for the inlets with an external supersonic diffuser regardless of the inlet type.
- The streamline-traced inlets have much lower wave drag than the other types of inlets.
- The use of a strong oblique terminal shock wave for the two-dimensional inlets for freestream Mach number of $M_0$ = 2.0 resulted in reduced wave drag than two-dimensional inlets using a normal terminal shock wave.
- The streamline-traced inlets had 1 to 3% percent greater spillage than the other inlets, which was compensated by increasing the size of the capture area.
- The total pressure radial and distortion indices were within their limits at the design condition. The use of vortex generators within the subsonic diffuser could reduce distortion further below the limit.
- The axisymmetric spike inlet is an attractive inlet for Mach 1.4 to 1.7 due to its better performance, compact size, and likely stable shock wave system.
- For Mach 1.7 to Mach 2.0, the streamline-traced inlets appeared superior compared to the axisymmetric spike inlets due to their lower wave drag. However, off-design performance may reduce the advantages of the streamline-traced inlets.

The data of this study provide information for the selection of the inlet type and their expected level of performance. Work will continue to further refine the inlets, as well as investigate off-design performance including angle-of-sideslip, operation at subsonic speeds, and integration with a wing or aircraft.


## Acknowledgments

This work was funded by the Commercial Supersonic Technology (CST) Project of the NASA Advanced Air Vehicles Program.

## References


[1] Berton, J. J., Huff, D. L., Seidel, J. A., and Geiselhart, K. A., “Supersonic Technology Concept Aeroplanes for Environmental Studies,” AIAA Paper 2020-0263, January 2020.

[2] Slater, J. W., “Design Factors for Two-Dimensional, External-Compression Supersonic Inlets,” AIAA Paper 2020-2090, January 2020.

[3] Howerton, L. W. and Slater, J. W., “Auxiliary Inlet Design Study for Mach 1.4,” AIAA Paper 2021-3548, August 2021.

[4] Slater, J. W., “Refinement of Vortex Generators in a Streamline-Traced, External-Compression Supersonic Inlet,” AIAA Paper 2019-4423, August 2019.

[5] Slater, J. W., “Streamline-Traced, External-Compression Supersonic Inlets for Mach 2”, ISABE Paper 2022-0278, September 2022.

[6] Slater, J. W., “A Study of the Internal Aerodynamics of the Concorde Inlet,” AIAA Paper 2020-3770, August 2020.

[7] Slater, J. W., “Supersonic External-Compression Inlets for Mach 1.4 to 2.0,” AIAA Paper 2023-4016, June 2023.

[8] Slater, J. W., “Off-Design Analysis of Axisymmetric External-Compression Supersonic Inlets for Mach 1.4 to 2.0,” ISABE Paper 2024-022, September 2024.

[9] Slater, J. W., “SUPIN: A Tool for the Aerodynamic Design and Analysis of Supersonic Inlets,” NASA TM 20240008586, October 2024.

[10] Society of Automotive Engineering (SAE), “Aircraft Propulsion System Performance Station Designation and Nomenclature,” Aerospace Standard (AS) 755, December 1997.

[11] Otto, S. E, Trefny, C. J. and Slater, J. W., “Inward-Turning Streamline-Traced Inlet Design Method for Low-Boom, Low-Drag Applications,” *AIAA Journal of Propulsion and Power*, Vol. 32, No. 5, 2016, pp. 1178-1189.

[12] Walatka, P. P., Buning, P. G., Pierce, L., and Elson, P. A., “PLOT3D User’s Manual,” NASA-TM-101067, March 1990.

[13] Yoder, D. A., ‘Wind-US User’s Guide: Version 3.0,” NASA TM 2016-219078, March 2016.

[14] Menter, F. R., “Two-Equation Eddy-Viscosity Turbulence Models for Engineering Applications,” *AIAA Journal*, Vol. 32, No. 8, 1994, pp. 1598–1605. doi: 10.2514/3.12149.

[15] Society of Automotive Engineers (SAE), “Gas Turbine Engine Inlet Flow Distortion Guidelines,” SAE ARP 1420, Rev. C, April 2017.

[16] Bowditch, D. N., Coltrin, R. E., Sanders, B. W., Sorensen, N. E., and Wasserbauer, J. F., “Supersonic Cruise Inlets,” *Aircraft Propulsion*, NASA SP-259, November 1970.

[17] Hirt, S. M., Chima, R. V., Vyas, M. A., Conners, T. R., Wayman, T. R., and Reger, R. W., “Experimental Investigation of a Large-Scale Low-Boom Inlet Concept,” AIAA Paper 2011-3796, June 2011.